# ESR/U-series and ESR dating of several Middle Pleistocene Italian sites: Comparison with 40Ar/39Ar chronology

Jean-Jacques Bahain, Pierre Voinchet, Amina Vietti, Qingfeng Shao, Olivier Tombret, Alison Pereira, Sébastien Nomade, Christophe Falguères

# ESR/U-series and ESR dating of several Middle Pleistocene Italian sites: comparison with $^{40}Ar/^{39}Ar$ chronology

Jean-Jacques BAHAIN [1*], Pierre VOINCHET [1], Amina VIETTI [1, 2], Qingfeng SHAO [3], Olivier TOMBRET [1], Alison PEREIRA [1,4,5,6 *], Sébastien NOMADE [4], Christophe FALGUÈRES [1]

[1]UMR 7194 HNHP Histoire naturelle de l'Homme préhistorique, MNHN-CNRS-UPVD, Département Homme et Environnement du Muséum national d'Histoire naturelle, Institut de Paléontologie Humaine, 1 rue René Panhard, 75013, Paris France

[2]Dipartimento di chimica, Università degli Studi di Torino, 10125 Turin, Italy

[3]College of Geographical Science, Nanjing Normal University, Nanjing 210023, China

[4]Laboratoire des Sciences du Climat et de l'Environnement, LSCE/IPSL, CEA-CNRS-UVSQ, Université Paris-Saclay, F-91191 Gif-sur-Yvette, France

[5]Ecole française de Rome, Piazza Farnese, IT-00186, Roma, Italy

[6]Sezione di Scienze Preistoriche e Antropologiche, Dipartimento di Studi Umanistici, Università degli Studi di Ferrara, C.so Ercole d'Este I, 32, Ferrara, Italy

* present adress : UMR 8148 GEOPS Laboratoire Géosciences Paris-Sud, Université Paris-Saclay-CNRS, Campus Vallée, Rue du Belvédère, Bâtiment 504, 91400 Orsay, France

**Abstract**

The stratigraphic sequences of numerous Palaeolithic sites of Central and Southern Italy, very rich in both archaeological and palaeontological remains, have also recorded Pleistocene volcanic events through volcanic ash deposits (tephra). They allow the establishment of an accurate chronological framework by comparing results obtained by $^{40}Ar/^{39}Ar$ dating method on single volcanic K-feldspar crystals, with those derived from ESR and ESR/U-series analyses on fluvial bleached quartz and tooth enamel respectively.

Since 2009, these three methods were hence applied on samples of several Middle Pleistocene sites of Central and Southern Italy including both volcanic and archaeological levels (from the west to the east): La Polledrara di Cecanibbio, Isoletta, (Latium), Guado San Nicola, Isernia La Pineta (Molise), Valle Giumentina (Abruzzo) and Venosa Notarchirico (Basilicata).

The obtained results, covering a time range from 350 to 660 ka, prove that such a multi-method approach when possible is essential to constrain the chronology of each site and allow the recognition of the specific limitations due to the lack of quartz for ESR or to complex geochemical histories in teeth rendering difficult the ESR /U-series meth-

od. Despite these limitations, the ESR framework is globally in agreement with the $^{40}Ar/^{39}Ar$ chronology, while ESR/U-series dates can be underestimated for the oldest sites. In such cases, an isochron approach attests however of the quite good reliability of the palaeodosimetric reconstruction and the observed age underestimation could be related to other factors affecting the ESR age determination.

Key-words – ESR/U-series dating, ESR dating, $^{40}Ar/^{39}Ar$ dating, Middle Pleistocene, Palaeolithic, Italy

---

**Introduction**

The dating of Middle Pleistocene archaeological sites can usually be performed using a relatively restricted number of geochronological methods. The opportunity to use these technics relies on both the considered time range and available datable materials found on these sites. These parameters greatly depend on the geological context and, consequently, the establishment of accurate chronological framework of the Middle Pleistocene human evolutionary scheme is very heterogeneous in terms of precision and accuracy in the various areas of the world. In Western Europe, this framework was mainly built by uranium-series (U-series) dates on speleothems and by palaeodosimetric dating methods such as thermoluminescence (TL) on heated flints, optically stimulated luminescence (OSL) on sediments, electron spin resonance (ESR) on fluvial sediments and coupled ESR and U-series on teeth. For open-area localities, at least one of these palaeodosimetric methods can generally be applied but, if several methods are used at the same time and show geochronological discrepancy, the lack of completely independent age control drastically complicates the chronological and archaeological interpretation.

However, it is possible in some areas of the European continent to benefit of the combine application of independent dating methods. It is the case in Central and Southern Italy where the stratigraphic sequences of numerous Palaeolithic sites, very rich in both archaeological and palaeontological remains, contain tephra deposits and record hence the regional volcanic history. The study of such sequences allows hence the comparison of the chronologies derived from ESR and ESR/U-series analyses on fluvial bleached quartz and tooth enamel respectively with the chronological framework obtained by $^{40}Ar/^{39}Ar$ dating method on single volcanic K-feldspar crystals. The $^{40}Ar/^{39}Ar$ method became a reference method for the Quaternary chronology as evidenced by the geochronological framework of human evolution in East Africa that was established thanks to this technic (see for example Brown et al., 2012 or McDougall, 2014).

In 2009, in collaboration with Italian and French archaeologists and geologists, we initiated an inter-comparison geochronological project aiming to date by different methods Middle Pleistocene sites of Central and Southern Italy,

which displayed both volcanic materials and archaeological levels. On each site, teeth and sediments containing volcanic minerals, both in primary fallout deposits and in reworked sedimentary layers, as well as sediments containing quartz when present, were systematically sampled. The main results obtained in this inter-comparison project are displayed in this paper and compared to the data derived from paleo-environmental and geological studies in order to improve the chronology of the sites dated by only one method or/and only from the available paleo-environmental data. The present paper synthetizes hence for the first time the data obtained during the project by ESR/U-series and ESR on these Italian sites and compares them with the $^{40}Ar/^{39}Ar$ chronology established in parallel for each site, allowing a general discussion on the potential and limits of ESR/U-series and ESR technics applied to date Middle Pleistocene sites. Even if the main part of the displayed results are already published in different papers, the main issue of the present methodological article is to compare systematically the dating results obtained by ESR/U-series and ESR with those derived from $^{40}Ar/^{39}Ar$ analyses, such systematic discussion with comparison having not really realized before.

**Sites, sampling and $^{40}Ar/^{39}Ar$ chronology**

From the west to the east, the studied sites are La Polledrara di Cecanibbio, Isoletta, Lademagne (Latium), Guado San Nicola, Isernia La Pineta (Molise), Valle Giumentina (Abruzzo) and Notarchirico (Basilicata) (Figure 1). The stratigraphic sequences of these sites, display both archaeological levels with, for some of them, abundant palaeontological fossils, and either primary volcanic deposits such as tephra, or fluvial or fluvio-lacustrine deposits rich in fresh volcanic minerals reworked from such primary volcanic deposits (Figure 2).

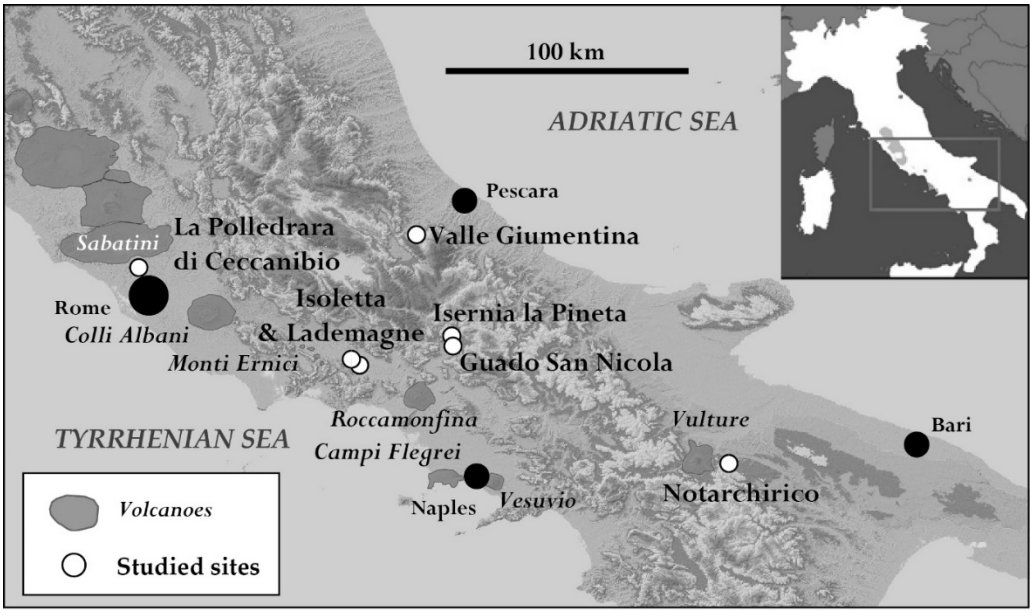


**Figure 1** - Location of the studied Middle Pleistocene sites in Central and Southern Italy.

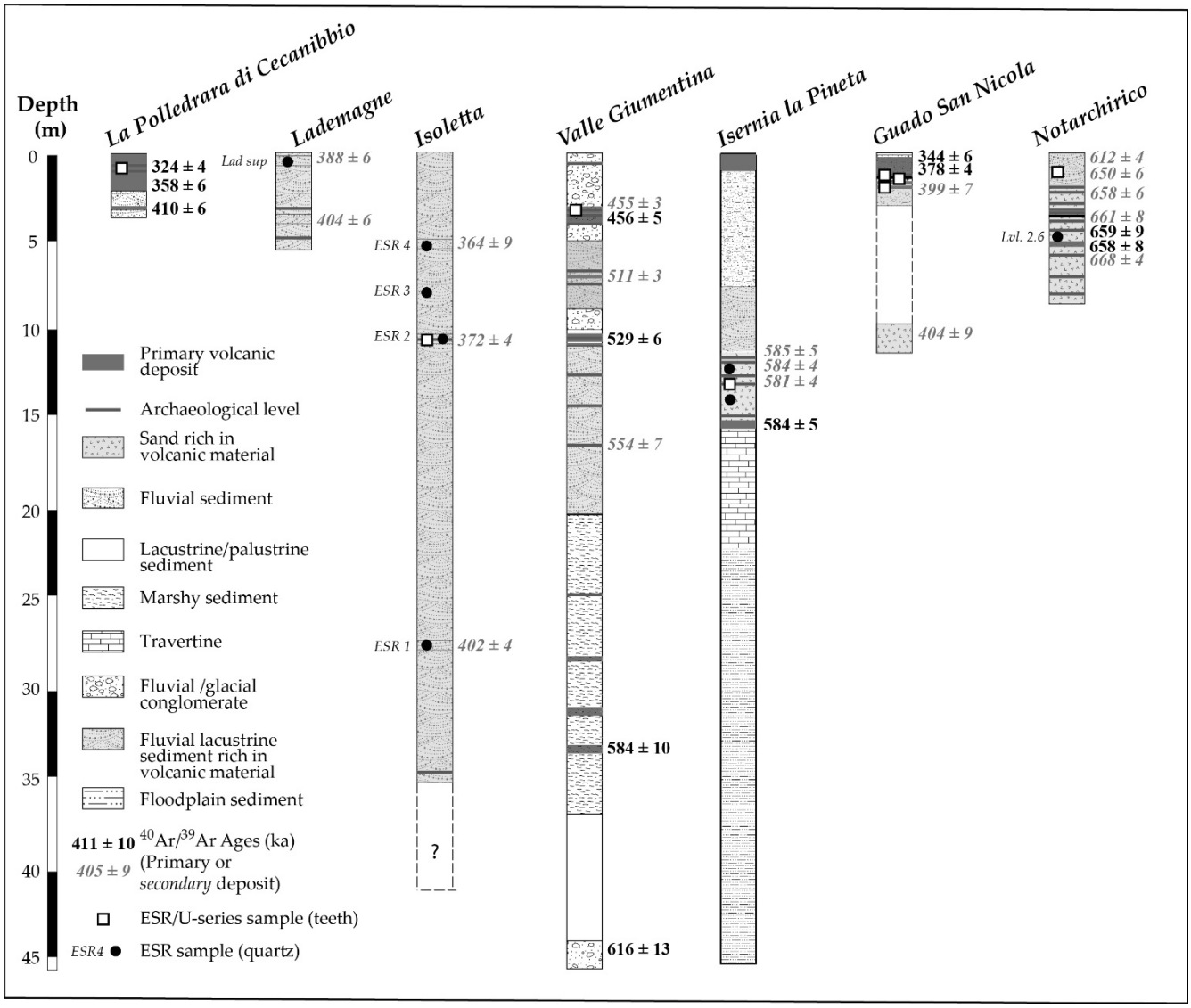


**Figure 2 –** Simplified stratigraphic logs of the studied Middle Pleistocene sites with indication of the levels dated by $^{40}Ar/^{39}Ar$ and positions of the levels sampled for ESR and ESR/U-series studies. $^{40}Ar/^{39}Ar$ ages were obtained directly on tephra levels (primary deposits) or on potassic feldspar grains extracted from fluvial sediments (secondary deposits), the youngest population corresponding then to a maximum age for the dated level.

La Polledrara di Cecanibbio is located only at 20 km from Rome. Discovered in 1984, the site is since excavated yearly and it is currently considered as one of the richest palaeontological and archaeological deposits of the Latium province, Latium (Anzidei et al., 2004, 2012; Santucci et al., 2016). More than 20 000 palaeontological remains, constituting an assemblage attributed to the Aurelian Large Mammal's stage of the Italian bio-chronological sequence (Palombo and Milli, 2005, Marra et al., 2018; Petronio et al., 2019), and at least 600 artefacts were recovered in fluvial and volcanic lahar sediments rich in pyroclastic minerals originated from the Monti Sabatini volcanic complex. Three different stratigraphic layers and seven *Bos primigenius* teeth were sampled for $^{40}Ar/^{39}Ar$ on single grain and ESR/U-series dating methods respectively (Pereira et al., 2017).

Isoletta and Lademagne sites are both located 110 km southeast of Rome in the Frosinone-Ceprano tectonic basin of the Latina Valley, close to the Campogrande locality where was discovered in 1994 the Ceprano human calvarium (Ascenzi et al., 1996, Manzi et al., 2016). Both sequences include mainly fluvial deposits rich in volcanic materials, some tephra layers being deposited also at Isoletta, and several archaeological layers displaying for the upper one Acheulean artefacts (Biddittu, 2004; Biddittu et al., 2012). Several fluvial levels were sampled at Lademagne (n=2) and Isoletta (n=4) for both ESR and $^{40}Ar/^{39}Ar$ analyses as well as a cervid tooth from the Acheulean level of Isoletta (Pereira et al., 2018; Voinchet et al., 2020).

Isernia La Pineta, 180 km southeast of Rome, is one of the most famous and ancient palaeolithic sites of Italy. It was extensively excavated since its discovery in 1978 and has delivered abundant lithic and faunal remains characteristic of the Middle Galerian Large Mammal's stage. The site was found in a complex stratigraphic sequence including lacustrine, volcanic, fluvial and slope deposits (Coltorti et al., 1982; Peretto et al., 1983, 2015a). A volcanic unit at the base of the archaeological sequence and four teeth (bison and rhinoceros) from the main archaeological unit t3c were sampled as well as sediments (n=2) from the archaeological sequence (Shao et al., 2011; Peretto et al., 2015).

The Guado San Nicola site, only 10 km south of Isernia, was discovered in 2005. It site was excavated between 2008 and 2012 allowing the recovering of more than 4000 lithic artefacts and 1500 faunal remains. The palaeontological assemblage is characteristic of the final Italian Galerian stage while the lithic industry includes both Mode 2 and Mode 3 artefacts (Peretto et al., 2016). The archaeological layers are included into a fluvial sequence covered by several volcanic units attributed to the Roccamonfina volcanic complex (Peretto et al., 2014, 2016). Three different layers of the stratigraphic sequence (tephra and fluvial deposits) and six teeth (horses and rhinoceros) were sampled for $^{40}Ar/^{39}Ar$ and ESR/U-series (6 teeth in total) dating methods respectively (Peretto et al., 2016; Pereira et al., 2016).

Valle Giumentina is located about 120 km east of Rome and displays a 70m thick sedimentary sequence, mainly constituted by lake shore deposits, in which were found several Palaeolithic levels attributed to the Clactonian and Acheulean in the lower part of the sequence and Levalloisian cultures In the uppermost part respectively (Demangeot and Radmilli, 1953; Nicoud et al., 2015). Numerous tephra layers were also recognized in the stratigraphic (Nicoud et al., 2015; Villa et al., 2016; Degeai et al., 2018). Seven of these volcanic primary deposits sampled all along the sequence and one cervid tooth extracted from a mandible carried out from an Acheulean level (ALB-42) were dated (Nicoud et al., 2015; Villa et al., 2016; Degeai et al., 2018).

Lastly, the early Middle Pleistocene site of Notarchirico is one of the most famous archaeological localities of Southern Italy (Piperno, 1997; Lefèvre et al., 2010). Located 180 km east of Naples close to Monte Vulture stratovolcano, the site is constituted by a 7m-thick fluvial sequence including eleven archaeological layers. Some of these archaeo-surfaces have delivered handaxes considered as the oldest evidence of Acheulean settlement presently known in Italy (Pereira et al., 2015) and one human femur attributed to *Homo heidelbergensis* (Mallegni et al., 1991). A tephra layer in the lower part of the sequence and several fluvial sediments reworking volcanic minerals were sampled for $^{40}Ar/^{39}Ar$, as well as three quartz-rich levels (unit 2.6) and four teeth from the upper palaeoanthropological layer (supra-α) for ESR and ESR-U-series methods respectively (Voinchet et al., 2020).

Details on the analytical $^{40}Ar/^{39}Ar$ protocol applied on single volcanic K-feldspar crystals and the main part of the results have been already published in detail (Pereira et al., 2015, 2016, 2017, 2018; Peretto et al., 2015, Villa et al., 2016). These data have permitted to greatly refine the chronology of the studied stratigraphic sequences and associated archaeological levels of the sites.

In the present paper, $^{40}Ar/^{39}Ar$ ages are presented as weighted mean ages with related full external error at 2σ (analytical + decay constant uncertainties) and as plotted from an inverse isochron diagram ($^{36}Ar/^{40}Ar$ vs $^{39}Ar/^{40}Ar$). Such diagram permits to assess the isotopic composition of $^{40}Ar$ trapped at the time of crystallization of the dated minerals and hence evaluate the possibility of argon excess by verifying the assumption that trapped argon isotopes at the eruption time presented the composition of modern atmosphere ($^{40}Ar/^{36}Ar$ ratio of 298.56 (Lee et al., 2006)). Ages were re-calculated in the present contribution according the monitor flux standard ACs-2 at 1.1891 Ma (Niespolo e al., 2017) and the K total decay constant of Renne et al. (2011). If the dated samples do not show evidence of such contamination, the calculated inverse isochron age should be equivalent to the weighted mean average one. Inverse isochron $^{40}Ar/^{36}Ar$ initial ratio as well as the related calculated ages at 2σ of uncertainties will be therefore displayed.

**ESR and ESR/U-series geochronological studies**

*ESR dating on optically bleached quartz*

In the case of ESR dating of fluvial quartz grains, the dated event corresponds to the sediment deposition by the river after the exposure of the quartz grains to the sunlight during the river transport phase prior to this deposition. This exposure leads to an optical bleaching of the quartz ESR signals.

In the present work, both aluminium (Al) and titanium (Ti) impurity centers are used for dating purpose. It is important to keep in mind that the different Ti signals associated to lithium (Ti-Li) and hydrogen (Ti-H) atoms occurrence in the vicinity of titanium ones can be quickly and completely reset by light exposure which is not the case of Al-signals, probably because of the presence in quartz aluminium centers of “Deep Aluminium Traps” (DAT) that cannot be emptied by the energy provided by sunlight (Tissoux et al 2013). It is therefore necessary to determine for each sample the level of "residual" ESR signal intensity, corresponding to the maximum bleaching of the Al-centers into the quartz grains, by exposure of the quartz grains to artificial solar light in the simulator for ca 1600 hours. The “unbleachable” ESR intensity hence obtained subtracted from the ESR signal intensities of the other aliquots of the same sample (including natural one) before the construction of the growth curve prior to any age calculation.

An multi-center ESR approach, based on the systematic measurements of both aluminium (Al), titanium-lithium (Ti-Li) and titanium-hydrogen (Ti-H) signals (Toyoda et al., 2000), was therefore used to date the quartz samples. This method relies on the differences of sensibility of these ESR centers to light. While Ti centers are totally zeroed by sunlight exposure within few hours (Ti-H) or days (Ti-Li), Al-center cannot be completely reset even after several months of exposure. In these conditions, the results obtained for a same sample from these three ESR signals permit to discuss of the quality of the initial bleaching of the quartz grains before deposition on the site or to indicate contaminations by unbleached quartz grains from older levels or bedrock (Duval and Guilarte, 2015 ; Voinchet et al., 2020).

Preparation and measurement protocols used during the present work have been recently displayed by Voinchet et al. (2020). Several sampled sediments did not contain enough quartz to allow an analysis and only 6 quartz samples have been finally analysed: 4 from Isoletta, 1 from Lademagne and 1 from Notarchirico. The equivalent doses and derived ages were calculated from Al- and Ti-centers for all the samples except Notarchirico sample, which not displayed any Ti-signals, and Lademagne one, for which it was not possible to measure Ti-H signal, undistinguishable to the ESR background noise. For the other samples, the multi-center approach was therefore used. When $D_E$ values obtained from the different centers of a sample were close, a weighted average age was calculated using IsoPlot 3.0 (Ludwig, 2003) with 95 % of confidence.

*ESR/U-series on teeth*

In the present work, the analysed teeth corresponds to herbivorous cheek teeth (molars or premolars), mainly from bovids bust also from equids, rhinoceros and cervids (Table 1).

| Site | Sample | Sample laboratory number | Type of analysed tooth |
|---|---|---|---|
| La Polledrara di Cecanibbio | Po2012-01 | IPH-2012-51 | Cheek tooth Bovidae |
| | Po2012-02 | IPH-2012-52 | Cheek tooth Bovidae |
| | Po2012-03 | IPH-2012-53 | Cheek tooth Bovidae |
| | Po2012-04 | IPH-2012-54 | Cheek tooth Bovidae |
| | Po2012-05 | IPH-2012-55 | Cheek tooth Bovidae |
| | Po2012-06 | IPH-2012-56 | Cheek tooth Bovidae |
| | Po2012-07 | IPH-2012-57 | Cheek tooth Bovidae |
| Guado San Nicola | SN1001 | IPH-2010-14 | Cheek tooth Bovidae |
| | SN1002 | IPH-2010-15 | Cheek tooth Bovidae |
| | SN0902 | IPH-2009-27 | Cheek tooth Equidae |
| | SN0906 | IPH-2009-31 | Cheek tooth Bovidae |
| | SN1003 | IPH-2010-16 | Cheek tooth Rhinocirotidae |
| | SN1004 | IPH-2010-17 | Cheek tooth Rhinocirotidae |
| Isoletta | ISOL1401 | IPH-2014-28 | Cheek tooth Cervidae |
| Valle Giumentina | VG1501 | IPH-2015-04 | Cheek tooth Cervidae |
| Isernia la Pineta | IS0901 | IPH-2009-01 | Cheek tooth Bovidae |
| | IS0902 | IPH-2009-02 | Cheek tooth Bovidae |
| | IS0903 | IPH-2009-03 | Cheek tooth Bovidae |
| | IS0904 | IPH-2009-04 | Cheek tooth Bovidae |
| Venosa Notarchirico | VN1201 | IPH-2012-38 | Cheek tooth Rhinocirotidae |
| | VN1202 | IPH-2012-39 | Cheek tooth Rhinocirotidae |
| | VN1203 | IPH-2012-40 | Cheek tooth Bovidae |
| | VN1204 | IPH-2012-41 | Cheek tooth Bovidae |

**Table 1** – List and nature of the analysed teeth from several Middle Pleistocene Italian sites

Post-mortem uranium-uptake into the dental tissues leads to the variation of the dose rate over time. This phenomenon, which depends on the nature of the site and the age of the sample, makes the determination of the ESR ages, strongly linked to uranium content, particularly delicate and it is necessary to use mathematical models to describe the evolution of this parameter over time. In order to calculate the age of a given sample, the various data acquired through ESR and U-series analyses are then used to model post-mortem U-uptake in the different tissues followed in some cases by a loss of uranium (leaching) in order to provide an unique age. One of the main interests of this approach is to allow the determination for each dental tissue of a U-uptake parameter calculated from the whole set of analytical data and hence the description of the uranium-uptake kinetics into the considered tissue.

The mathematical algorithm for calculating combined ESR/U-series ages has been recently described by Shao et al. (2014). From the U-series isotopic data (U contents, isotopic ratios $^{234}U/^{238}U$, $^{230}Th/^{234}U$, $^{222}Rn/^{230}Th$), a relationship between the incorporation parameter and time is first determined for each dental tissue. It then becomes possible to simulate the evolution over time of the contributions of the different dental tissues to the dose rate. By adding the simulation of the environmental external dose, it becomes possible to simulate the evolution of the total dose rate over time and then to calculate an age by comparing the $D_E$ value obtained experimentally by ESR with this simulation. From this age, a single value corresponding to the incorporation parameter can be calculated for each

196 tissue. In the case of a simple U-uptake, the age is determined with the *Uranium-series* (US) *model* (Grün et al.,
197 1988), while in the case of a subsequent slight leaching, the U-uptake can be described with the *accelerating uptake*
198 (AU) *model* (Shao et al., 2012).

199 It should also be underlined that the main part of the results discussed in the present paper have been soon pub-
200 lished in previous papers (La Polledrara di Cecanibbio, Pereira et al., 2017; Guado San Nicola, Bahain et al., 2014,
201 Pereira et al., 2016; Isernia la Pineta, Shao et al., 2011 ; Isoletta, Pereira et al., 2018) and only results of Venosa No-
202 tarchirico (4 samples) and Valle Giumentina (one sample) are completely unpublished data.

203

204 *Isochron ESR/U-series dating of teeth*

205 The use of isochrons in teeth ESR dating was proposed in 1993 by Bonnie A. Blackwell and Henry P. Schwarcz to
206 take into account a possible variation of the external dose over time in the age calculation using fixed of U-uptake
207 models (Blackwell and Schwarcz, 1993). If it is assumed that the external dose has not varied over time, a diagram
208 can be drawn showing the equivalent doses determined for several sub-samples of the same tooth as a function of
209 the annual internal dose determined for the same sub-samples using the considered U-uptake model (*isochron*). If
210 the points of this isochron are linearly correlated, then the slope of the regression gives the age of the tooth and its
211 intercept with the y-axis gives the accumulated external dose common to all sub-samples. The procedure can then
212 be repeated for other external dose values until the best possible correlation between the data is obtained for a
213 given incorporation pattern. It then becomes possible to discuss the appropriateness of using one intake pattern
214 relative to another for the samples under consideration (Blackwell and Schwarcz, 1993; Blackwell et al., 2001). Very
215 cumbersome to implement and very time-consuming, this approach has unfortunately been little used thereafter.

216 More recently, a slightly modified isochronous approach was used to judge the relevance of the dosimetric re-
217 construction carried out on samples from the Middle Paleolithic site of Biache-Saint-Vaast, France (Bahain et al.,
218 2015). In this study, several teeth of the same level excavated in the 1980s were dated by ESR/U-series, using for the
219 external dose an *in situ* value measured during the excavation as the site is no longer accessible today. Two age
220 groups were then individualized for the analysed teeth, although the archaeological level is very homogeneous from
221 a paleontological point of view and a mixture of two stocks of different ages seems unlikely.

222 A diagram showing the equivalent dose values as a function of the total internal dose modelled by ESR/U-Th for
223 samples assumed to be of the same age *(isochron plot*) was therefore produced. As the data were highly linearly
224 correlated, it was possible to confirm on the one hand the relevance of using the in situ external dose measured

during the excavation and on the other hand to estimate the age of the level under consideration using the equation of the regression line obtained. The intercept of this line with the Y-axis then corresponds to the proportion of the equivalent dose linked to the external dose. By dividing this value by the annual external dose determined today for the level under consideration, it is possible to estimate the isochron age of the latter and to compare it with the other available geochronological data.

Isochron estimates was also applied successfully on La Polledrara samples (Pereira et al., 2017), leading to a more systematic use on other Italian Middle Pleistocene sites when the number of analysed samples allow such use. In the present work isochron age estimates were therefore determined from Guado San Nicola, Isernia and Notarchirico samples.

**Results**

Results are displayed by methods in Tables 2 ($^{40}Ar/^{39}Ar$), 3 (ESR), 4 and 5 (ESR/U-series) but will be discussed site by site from the youngest one (La Polledrara) to the oldest one (Notarchirico). The $^{40}Ar/^{39}Ar$ results permit to constrain the ages of the dated archaeological sequences and therefore the ages of associated ESR/U-series and ESR samples.

Concerning the ESR dating of quartz grains (Table 3), except for Isoletta ESR 1 sample for which the age is drastically overestimated for both Al and Ti centers, the age estimates derived from both signals for the other samples are globally in agreement with each other and with the $^{40}Ar/^{39}Ar$ ages obtained for the corresponding levels (Voinchet et al., 2020). While the number of samples is too small to allow a definitive conclusion on this point, these results suggest that the ESR multi-center protocol used here permit to obtain reliable chronology for Middle Pleistocene fluvial sediments. The dose rate was calculated from the radionuclides activities derived both from *in situ* gamma-ray spectrometry measurements using NaI detector and laboratory high resolution and low background gamma spectrometer using a hyper-pure Ge crystal.

| Site | Sample | Stratigraphical location of analysed samples | $^{40}Ar/^{39}Ar$ ages (ka) | Mean Square Weighted Deviation | Probability fit | Isochron ages (ka) | $^{40}Ar/^{36}Ar$ initial ratio |
|---|---|---|---|---|---|---|---|
| **La Polledrara di Cecanibbio** (Pereira et al., 2017) | POL 1203 &1201 | Pumices inside the archaeological level | **324 ± 4** | 0.7 | 0.9 | **323 ± 7** | 296 ± 3 |
| | POL1202 | Pumices from fluvial deposit just below archaeological level | **358 ± 6** | 0.8 | 0.5 | **368 ± 18** | 249 ± 80 |
| | POL1301 | Tephra 1m below archaeological level | **410 ± 6** | 0.3 | 1.0 | **410 ± 6** | 295 ± 9 |

| | | | | | | | | |
|---|---|---|---|---|---|---|---|---|
| **Guado San Nicola** (Pereira et al., 2016) | S.U. tufi | Volcanic level at the top of the sequence | **344 ± 6** | 0.2 | 0.6 | **339 ± 15** | 299 ± 8 |
| | S.U. A | Volcanic level just capping the archaeological sequence | **378 ± 4** | 1.0 | 0.4 | **376 ± 5** | 307 ± 11 |
| | S.U. C | Fluvial deposits inside the Lower archaeological level | **399 ± 7** | 0.5 | 0.9 | **400 ± 6** | 292 ± 15 |
| | Volcanic sands | Fluvial deposits 10m below the archaeological sequence | **404 ± 9** | 1.3 | 0.2 | **405 ± 10** | 282 ± 11 |
| **Isoletta** (Pereira et al., 2018) | ESR 4 | Fluvial deposits 5m above the Acheulean archaeological level | **364 ± 9** | 0.3 | 0.8 | **/** | / |
| | GA6Z | Sediments of the Acheulean archaeological level | **374 ± 4** | 1.4 | 0.2 | **374 ± 4** | 298 ± 2 |
| | ESR 1 | Fluvial sands at the bottom of the studied sequence | **402 ± 4** | 0.9 | 0.6 | **400 ± 10** | 300 ± 4 |
| **Lademagne** (Pereira et al., 2018) | LAD sup | Sediments at the top of the archaeological sequence | **388 ± 6** | 1.6 | 0.1 | **390 ± 7** | 289 ± 11 |
| | LAD inf | Sediments from a layer located between two archaeological levels | **404 ± 6** | 1.1 | 0.4 | **405 ± 7** | 293 ± 6 |
| **Valle Giumentina** (Nicoud et 116 al., 2015; Villa et al., 2016; Degeai et al., 2018) | T103b | Sediments of the archaeological level LABM | **455 ± 3** | 0.7 | 0.7 | **454 ± 3** | 297 ± 3 |
| | T109b | Sediments of the archaeological level LAN2 | **529 ± 6** | 1.3 | 0.3 | **528 ± 6** | 300 ± 3 |
| | T115 | Sediments of the archaeological level LN | **554 ± 7** | 0.6 | 0.8 | **554 ± 6** | 294 ± 1.4 |
| | T32 | Tephra below the archaeological sequence | **584 ± 10** | 0.4 | 0.9 | **581 ± 17** | 305 ± 30 |
| | T45 | Tephra at the bottom of the sedimentary sequence | **616 ± 13** | 0.2 | 1.0 | **617 ± 14** | 298 ± 4 |
| **Isernia la Pineta** (Peretto et al., 2015) | 3s6-9 | Sediments sampled above the main archaeological level t3a | **585 ± 5** | 1.0 | 0.5 | **585 ± 5** | 291 ± 7 |
| | 3s10 | Sediments sampled above the main archaeological level t3a | **581 ± 7** | 1.4 | 0.2 | **581 ± 8** | 296 ± 4 |
| | 3coll | Sediments capping the main archaeological level t3a | **581 ± 4** | 1.2 | 0.3 | **583 ± 5** | 290 ± 10 |
| | U4T | Tephra just below the archaeological sequence | **584 ± 5** | 0.5 | 1.0 | **583 ± 7** | 305 ± 30 |
| **Venosa Notarchirico** (Pereira et al., 2015; Voinchet et al., 2020) | NOT1.6 | Top of the archaeological sequence | **612 ± 4** | 1.5 | 0.2 | **612 ± 4** | 296 ± 2 |
| | NOT 1.5 | Sediments capping supra α level | **650 ± 6** | 0.6 | 1.1 | **651 ± 6** | 295 ± 3 |
| | NOT 1.3 | Just below supra α level | **658 ± 6** | 0.1 | 1.2 | **657 ± 11** | 298 ± 36 |
| | NOT 2.6 | Just below D level | **661 ± 8** | 0.7 | 0.6 | **658 ± 9** | 294 ± 9 |
| | NOT 2.2 | Tephra between level E and F | **659 ± 9** | 0.3 | 1.0 | **663 ± 10** | 291 ± 6 |
| | NOT 2.1 | Tephra between level E and F | **658 ± 8** | 0.6 | 0.6 | **657 ± 8** | 304 ± 14 |
| | U.3 | Sediments just below F level | **668 ± 4** | 1.8 | 0.1 | **668 ± 4** | 297 ± 4 |

**Table 2** – $^{40}Ar/^{39}Ar$ ages obtained from volcanic minerals recovered from several Middle Pleistocene Italian sites.

The indicated $^{40}Ar/^{39}Ar$ age corresponds to the age of the youngest homogeneous potassic feldspars population. These ages were re-calculated in the present contribution according to the monitor flux standard ACs-2 at 1.1891 Ma (Niespolo e al., 2017) and the K total decay constant of Renne et al. (2011) from the original data published in the various referred papers. A homogeneous population is considered relevant when the weighted mean of these crystals has the following statistical characteristics: MSWD < 1.5, Probability fit ≥ 0.1. The weighted average ages were calculated using IsoPlot 3.0 (Ludwig, 2003) and given at 95% (2σ) of confidence.

| Site | Sample | ESR signal | $D_\alpha$ (µGy/a) | $D_\beta$ (µGy/a) | $D_\gamma$ (µGy/a) | $D_{cosmic}$ (µGy/a) | W (%) | $\delta_{bl}$ (%) | $D_a$ (µGy/a) | $D_E$ (Gy) | Age (ka) | Mean Age (ka) | $^{40}Ar/^{39}Ar$ Age (ka) |
|---|---|---|---|---|---|---|---|---|---|---|---|---|---|
| **Isoletta** (Pereira et al., 2018 ; Voinchet et al., 2020) | Isoletta ESR 1 | Ti-H | 19±1 | 190±11 | 168±10 | 24±1 | 15 | 100 | 401±15 | 325 ± 29 | 810 ± 47 | - | *402 ± 4* |
| | | Ti-Li | 19±1 | 190±11 | 168±10 | 24±1 | 15 | 100 | 401±15 | 715±75 | 1786 ± 327 | | |
| | | Al | 19±1 | 190±11 | 168±10 | 24±1 | 15 | 48 | 401±15 | 462±24 | 1154 ± 109 | | |
| | Isoletta | Ti-H | 57±2 | 1786±36 | 1008±28 | 33±2 | 14 | 100 | 2884±15 | 295 ± 20 | 102 ± 16 | 442±58 | *374 ± 4* |

| | | | | | | | | | | | | | |
|---|---|---|---|---|---|---|---|---|---|---|---|---|---|
| | ESR 2 | Ti-Li | 57±2 | 1786±36 | 1008±28 | 33±2 | 14 | 100 | 2884±15 | 1155±110 | 401 ± 59 | | |
| | | Al | 57±2 | 1786±36 | 1008±28 | 33±2 | 14 | 42 | 2884±15 | 1315±62 | 456 ± 34 | | |
| | Isoletta ESR 3 | Ti-H | 30±2 | 497±20 | 354±16 | 53±3 | 12 | 100 | 934±26 | 349±24 | 374±17 | 349±26 | *364 ± 9 < X < 374 ± 4* |
| | | Ti-Li | 30±2 | 497±20 | 354±16 | 53±3 | 12 | 100 | 934±26 | 314±73 | 336 ± 66 | | |
| | | Al | 30±2 | 497±20 | 354±16 | 53±3 | 12 | 46 | 934±26 | 338±60 | 362 ± 64 | | |
| | Isoletta ESR 4 | Ti-H | 20±1 | 303±12 | 220±10 | 101±5 | 15 | 100 | 644±16 | 243±15 | 374±84 | 396±83 | *364 ± 9* |
| | | Ti-Li | 20±1 | 303±12 | 220±10 | 101±5 | 15 | 100 | 644±16 | 275±25 | 426 ± 59 | | |
| | | Al | 20±1 | 303±12 | 220±10 | 101±5 | 15 | 45 | 644±16 | 252±40 | 391 ± 72 | | |
| **Lademagne** (Pereira et al., 2018 ; Voinchet et al., 2020) | Lademagne Sup | Ti-H | Unmeasurable | | | | | | | | | 402±71 | *388 ± 6* |
| | | Ti-Li | 77±3 | 980±35 | 919±52 | 111±6 | 5 | 100 | 2088±70 | 831±70 | 398 ± 51 | | |
| | | Al | 77±3 | 980±35 | 919±52 | 111±6 | 5 | 44 | 2088±70 | 847±100 | 406 ± 51 | | |
| **Venosa Notarchirico** (Pereira et al., 2015; Voinchet et al., 2020) | Level 2-6 | Ti-H | Unmeasurable | | | | | | | | | – | *612 ± 4 < X < 661 ± 8* |
| | | Ti-Li | Unmeasurable | | | | | | | | | | |
| | | Al | 84±1 | 1999±24 | 1803±21 | 166±8 | 10 | 57 | 4052±32 | 2660±122 | 657 ± 31 | | |

**Table 3** – ESR data and ages for sediments recovered from several Middle Pleistocene Italian sites.

Equivalent doses ($D_E$) were derived from the obtained intensity growth curves using an exponential + linear function for Al and Ti-Li centers (Duval et al., 2009; Voinchet et al., 2013) and by a single saturating exponential function for Ti-H from the six first points of the growth curves (Voinchet et al., 2020) with Microcal OriginPro 8 software, both with $1/I^2$ weighting (according with Yokoyama et al., 1985). Age calculations were performed using the following parameters: dose-rate conversions factors from Guérin et al. (2011); a k-value of 0.15 ± 0.1 (Laurent et al., 1998); alpha and beta attenuations from Brennan (2003) and Brennan et al. (1991); water attenuation formulae from Grün (1994); cosmic dose rate estimated from the Prescott and Hutton's equations (1994). The internal dose rate was considered as negligible because of the low contents of radionuclides usually found in quartz grains (Murray and Roberts 1997; Vandenbergue et al. 2008). ESR age estimates are given with one sigma error range.

Concerning the ESR/U-series results (Tables 4 and 5), when several teeth from a same archaeological level were analysed, the obtained age estimates are displayed both by age density probability plots and isochron plots (Figure 3) and are compared with the available $^{40}Ar/^{39}Ar$ and ESR dates (Figure 4). The age density plots build from the ESR/U-series age estimated with IsoPlot 3.0 software (Ludwig, 2003) permit to observe the homogeneity of the obtained age results and to determine mean ages for each eventual age populations. In complement, the isochron approach (Blackwell and Schwarcz, 1993) allows the evaluation of the quality of the dose rate reconstruction by comparison of the respective weight of accumulated external and internal dose contributions, the last one evolving with time according with the U-uptake modelling in each dental tissue. It permits to estimate an age estimate for a given level by plotting the accumulated internal doses modelled for the teeth *vs* the $D_E$ and by dividing the intercept value (x=0, that represents the corresponding accumulated external doses) by the "real" external dose rates used for the age calculation. These two graphic representations permit to better discuss of the results.

| Site | Samples | Tissue | U content (ppm) | $^{234}U/^{238}U$ | $^{230}Th/^{232}Th$ | $^{230}Th/^{234}U$ | Apparent U-series age (ka) | $^{222}Rn/^{230}Th$ | Initial thickness (µm) | Removed thickness Internal side(µm) | Removed thickness External side (µm) |
|---|---|---|---|---|---|---|---|---|---|---|---|
| La Polledra-ra di Cecanib-bio (Pereira et al., 2017) | Po2012-01 | dentine | 342.83 ± 9.12 | 1.215 ± 0.008 | 20 | 0.658 ± 0.030 | 112 ± 9 | 0.351 | 1270 ± 159 | 172 ± 21 | 32 ± 4 |
| | | enamel | 9.89 ± 0.26 | 1.131 ± 0.021 | > 100 | 0.760 ± 0.034 | 149+16/-13 | 0.612 | | | |
| | Po2012-02 | dentine | 294.18 ± 9.96 | 1.172 ± 0.033 | 48 | 0.617 ± 0.027 | 101 +8/-7 | 0.395 | 1323 ± 165 | 116 ± 14 | 6 ± 1 |
| | | enamel | 10.11 ± 0.33 | 1.148 ± 0.039 | 13 | 0.798 ± 0.039 | 164+23/-18 | 1.000 | | | |
| | Po2012-03 | dentine | 283.76 ± 8.81 | 1.215 ± 0.031 | > 50 | 0.575 ± 0.025 | 90+7/-6 | 0.390 | 1124 ± 140 | 191 ± 24 | 86 ± 11 |
| | | enamel | 23.52 ± 0.83 | 1.153 ± 0.044 | 46 | 0.629 ± 0.032 | 105+10/-9 | 0.321 | | | |
| | Po2012-04 | dentine | 326.73 ± 8.79 | 1.209 ± 0.026 | > 100 | 0.646 ± 0.026 | 108+8/-7 | 0.426 | 1394 ± 174 | 43 ± 5 | 114 ± 14 |
| | | enamel | 13.80 ± 0.49 | 1.387 ± 0.053 | > 50 | 0.704 ± 0.034 | 122+12/-11 | 0.497 | | | |
| | Po2012-05 | dentine | 273.00 ± 9.22 | 1.239 ± 0.036 | > 50 | 0.633 ± 0.033 | 105+10/-9 | 0.533 | 1238 ± 155 | 109 ± 14 | 78 ± 10 |
| | | enamel | 9.98 ± 0.28 | 1.185 ± 0.023 | > 50 | 0.699 ± 0.033 | 125+12/-11 | 0.557 | | | |
| | Po2012-06 | dentine | 340.53 ± 11.61 | 1.252 ± 0.034 | > 100 | 0.503 ± 0.027 | 74 ± 6 | 0.385 | 1339 ± 167 | 225 ± 28 | 155 ± 19 |
| | | enamel | 8.92 ± 0.25 | 1.164 ± 0.024 | > 100 | 0.679 ± 0.037 | 119+13/-12 | 0.650 | | | |
| | Po2012-07 | dentine | 396.22 ± 13.70 | 1.062 ± 0.030 | > 100 | 0.654 ± 0.035 | 114+12/-11 | 0.279 | 1376 ± 172 | 138 ± 17 | 75 ± 9 |
| | | enamel | 5.72 ± 0.24 | 1.473 ± 0.061 | > 100 | 0.724 ± 0.035 | 127+13/-11 | 0.780 | | | |
| Guado San Nicola (Bahain et al., 2014; Pereira et al., 2016) | SN1001 | cement | 40.76 ± 0.09 | 1.319 ± 0.004 | > 100 | *1.133 ± 0.008* | > 500 | 0.290 | 1053 ± 132 | 68 ± 8 | 12 ± 1 |
| | | dentine | 103.67 ± 0.45 | 1.253 ± 0.003 | > 100 | 0.950 ± 0.011 | 251 ± 12 | 0.407 | | | |
| | | enamel | 2.45 ± 0.01 | 1.303 ± 0.004 | 42 | 0.897 ± 0.011 | 207 ± 8 | 0.796 | | | |
| | SN1002 | cement | 108.95 ± 0.44 | 1.234 ± 0.004 | > 100 | 0.840 ± 0.007 | 180 ± 5 | 0.352 | 1204 ± 151 | 67 ± 8 | 13 ± 2 |
| | | dentine | 121.74 ± 0.45 | 1.248 ± 0.004 | > 100 | 0.831 ± 0.009 | 175 ± 6 | 0.352 | | | |
| | | enamel | 2.96 ± 0.01 | 1.281 ± 0.004 | > 50 | 0.765 ± 0.008 | 145 ± 4 | 0.705 | | | |
| | SN0902 | cement | 38.99 ± 0.11 | 1.319 ± 0.003 | > 50 | 1.167 ± 0.007 | > 500 | 0.307 | 1273 ± 159 | 32 ± 4 | 80 ± 10 |
| | | dentine | 140.33 ± 0.43 | 1.204 ± 0.003 | > 100 | 0.855 ± 0.005 | 190 ± 4 | 0.419 | | | |
| | | enamel | 3.38 ± 0.01 | 1.223 ± 0.005 | 100 | 0.786 ± 0.005 | 155 ± 3 | 0.662 | | | |
| | SN0906 | dentine | 67.27 ± 0.27 | 1.338 ± 0.006 | > 100 | *1.048 ± 0.010* | 365 ± 31 | 0.085 | 1793 ± 224 | 48 ± 6 | 58 ± 7 |
| | | enamel | 1.35 ± 0.01 | 1.254 ± 0.006 | 7 | *1.114 ± 0.010* | > 500 | 0.779 | | | |
| | SN1003 | dentine | 86.26 ± 0.21 | 1.328 ± 0.004 | > 100 | *1.055 ± 0.009* | 384 ± 31 | 0.363 | 2328 ± 291 | 56 ± 7 | 28 ± 4 |
| | | enamel | 0.50 ± 0.01 | 1.230 ± 0.006 | 3 | 0.934 ± 0.012 | 241 ± 14 | 0.790 | | | |
| | SN1004 | dentine | 83.68 ± 0.38 | 1.318 ± 0.003 | > 100 | *1.051 ± 0.010* | 379 ± 29 | 0.411 | 1896 ± 237 | 67 ± 8 | 40 ± 5 |
| | | enamel | 0.71 ± 0.01 | 1.402 ± 0.005 | 16 | 0.918 ± 0.011 | 213 ± 9 | 0.644 | | | |
| Isernia la Pineta (Shao et al., 2011) | IS0901 | cement | 120.33 ± 0.77 | 1.327 ± 0.009 | > 100 | 0.770 ± 0.018 | 146 ± 9 | 0.265 | 1098 ± 137 | 68 ± 9 | 108 ± 13 |
| | | dentine | 225.20 ± 1.07 | 1.314 ± 0.005 | > 100 | 0.720 ± 0.008 | 129 ± 3 | 0.255 | | | |
| | | enamel | 3.78 ± 0.02 | 1.355 ± 0.001 | 26 | 0.673 ± 0.023 | 114 ± 9 | 0.647 | | | |
| | IS0902 | dentine | 193.61 ± 0.95 | 1.276 ± 0.005 | > 100 | 0.695 ± 0.010 | 122± 4 | 0.250 | 1269 ± 159 | 153 ± 19 | 88 ± 11 |
| | | enamel | 3.25 ± 0.01 | 1.343 ± 0.001 | 12 | 0.691 ± 0.031 | 120 ± 2 | 0.479 | | | |
| | IS0903 | cement | 216.03 ± 1.04 | 1.253 ± 0.010 | > 50 | 0.621 ± 0.014 | 146 ± 9 | 0.182 | 1212 ± 151 | 115 ± 14 | 53 ± 7 |
| | | dentine | 237.29 ±1.07 | 1.263 ± 0.005 | > 100 | 0.574 ± 0.009 | 129 ± 3 | 0.238 | | | |
| | | enamel | 4.39 ± 0.01 | 1.320 ± 0.001 | 43 | 0.543 ± 0.016 | 82 ± 4 | 0.564 | | | |
| | IS0904 | cement | 126.93 ± 0.97 | 1.362 ± 0.013 | 22 | 0.901 ± 0.015 | 205 ± 13 | 0.173 | 1323 ± 165 | 243 ± 30 | 101 ± 13 |
| | | dentine | 201.84 ± 1.14 | 1.276 ± 0.005 | > 100 | 0.686 ± 0.009 | 119 ± 4 | 0.239 | | | |
| | | enamel | 2.62 ±0.01 | 1.343 ± 0.001 | 9 | 0.683 ± 0.037 | 118 ± 14 | 0.598 | | | |
| Venosa Notarchirico Level supra α (this work) | VN1201 | dentine | 246.25 ± 1.77 | 1.153 ± 0.009 | 20 | 0.892 ± 0.010 | 217 ± 8 | 0.972 | 1254 ± 157 | 283 ± 35 | 88 ± 11 |
| | | enamel | 3.19 ± 0.01 | 1.153 ± 0.001 | > 50 | 0.532 ± 0.002 | 81 ± 1 | 1.000 | | | |
| | VN1202 | dentine | 216.96 ± 1.68 | 1.164 ± 0.011 | 36 | 0.743 ± 0.012 | 141 ± 5 | 0.842 | 1469 ± 184 | 255 ± 32 | 58 ± 7 |
| | | enamel | 11.10 ± 0.04 | 1.174 ± 0.006 | 35 | 0.638 ± 0.005 | 107 ± 1 | 1.000 | | | |
| | VN1203 | cement | 158.83 ± 1.23 | 1.246 ± 0.008 | 25 | *1.020 ± 0.013* | 342 ± 26 | 0.733 | 1105 ± 138 | 92 ± 12 | 124 ± 16 |
| | | dentine | 197.72 ± 2.32 | 1.307 ± 0.012 | 39 | *1.056 ± 0.017* | 398 ± 54 | 0.638 | | | |
| | | enamel | 7.65 ± 0.04 | 1.307 ± 0.007 | 20 | 0.965 ± 0.008 | 256 ± 8 | 0.515 | | | |
| | VN1204 | dentine | 140.80 ± 0.73 | 1.458 ± 0.008 | > 50 | *1.078 ± 0.008* | 380 ± 21 | 0.679 | 1172 ± 146 | 190 ± 24 | 163 ± 20 |
| | | enamel | 5.77 ± 0.01 | 1.306 ± 0.003 | > 50 | *1.140 ± 0.004* | > 500 | 0.671 | | | |
| Isoletta (Pereira et al., 2018) | ISOL1401 | dentine | 109.86 ± 9.97 | 1.281 ± 0.027 | 31 | 0.865 ± 0.036 | 190 +23/-19 | 0.865 | 1078 ± 100 | 98 ± 12 | 67 ± 8 |
| | | enamel | 1.65 ± 0.07 | 1.316 ± 0.063 | > 100 | 0.953 ± 0.057 | 245 +76/-44 | 0.953 | | | |
| Valle Giumentina (this work) | VG1501 | dentine | 53.67 ± 1.67 | 1.426 ± 0.038 | > 50 | *1.078 ± 0.052* | > 300 | 0.898 | 1063 ± 100 | 118 ± 15 | 109 ± 14 |
| | | enamel | 1.60 ± 0.07 | 1.316 ± 0.060 | 4 | 1.058 ± 0.061 | > 300 | 0.364 | | | |

**Table 4** – U-series and ESR data for the analysed teeth recovered from several Middle Pleistocene Italian sites.

U-series analyses were performed on each dental tissue in order to determine the U-uptake parameters necessary to the dose rate contributions and age calculations (see details in Shao et al., 2015b), either by alpha spectrometry (MNHN, Paris), or by Neptune Multi-Collector Inductively Coupled Plasma Mass Spectrometer (MC-ICPMS) (Nanjing Normal University, China).

| Site | Samples | Tissue | $D_E$ (Gy) | U uptake parameters p (regular) or *n (italics)* | $D_a$ α internal (μGy/a) | $D_a$ β (μGy/a) | $D_a$ (γ + cosm) (μGy/a) | $D_a$ total (μGy/a) | ESR/U-series (US or AU) ages (ka) | $^{40}Ar/^{39}Ar$ ages, ESR/U-series density plot and ESR/U-series isochron age estimates (ka) |
|---|---|---|---|---|---|---|---|---|---|---|
| **La Polledrara di Cecanibbio** (Pereira et al., 2017) | **Po2012-01** | dentine<br>enamel | 1665 ± 169 | -0.360 ± 0.151<br>0.280 ± 0.248 | 1779 ± 868 | 708 ± 183 | 2716 ± 40 | 5203 ± 888 | **320 ± 44** | **$^{40}Ar/^{39}Ar$ age 324 ± 4**<br>**ESR/U-series density plot ages** Two populations 196 ± 25 (n=2) **324 ± 25 (n=4)**<br>**ESR/U-series isochron age** Two populations ≈ 153 (n=2) **≈321 (n=4)** |
| | **Po2012-02** | dentine<br>enamel | 1902 ± 105 | -0.593 ± 0.027<br>0.221 ± 0.172 | 2691 ± 696 | 1150 ± 212 | 2716 ± 40 | 6557 ± 729 | **290 ± 28** | |
| | **Po2012-03** | dentine<br>enamel | 1845 ± 141 | 0.208 ± 0.234<br>0.580 ± 0.287 | 2361 ± 487 | 1074 ± 52 | 2716 ± 40 | 6151 ± 702 | **300 ± 29** | |
| | **Po2012-04** | dentine<br>enamel | 1718 ± 48 | -0.683 ± 0.112<br>-0.538 ± 0.135 | 3008 ± 955 | 1902 ± 530 | 2716 ± 40 | 7626 ± 1093 | **183 ± 23** | |
| | **Po2012-05** | dentine<br>enamel | 1421 ± 89 | -0.076 ± 0.088<br>0.304 ± 0.114 | 1472 ± 314 | 1230 ± 200 | 2716 ± 40 | 5418 ± 375 | **317 ± 20** | |
| | **Po2012-06** | dentine<br>enamel | 1500 ± 104 | -0.128 ± 0.137<br>1.076 ± 0.263 | 1388 ± 528 | 863 ± 233 | 2716 ± 40 | 4968 ± 578 | **286 ± 28** | |
| | **Po2012-07** | dentine<br>enamel | 1248 ± 35 | -0.641 ± 0.068<br>-0.489 ± 0.084 | 1566 ± 338 | 1928 ± 360 | 2716 ± 40 | 6211 ± 495 | **201 ± 15** | |
| **Guado San Nicola** (Bahain et al., 2014; Pereira et al., 2016) | ***SN1001*** | *cement*<br>*dentine*<br>*enamel* | *1029 ± 31* | *-0.0051 ± 0.0005*<br>*-0.0042 ± 0.0005*<br>*-0.0038 ± 0.0005* | *643 ± 154* | *1211 ± 211* | *1560 ± 150* | *3408 ± 301* | ***302 ± 25*** | **$^{40}Ar/^{39}Ar$ ages 378 ± 4 < X < 399 ± 7**<br>**ESR/U-series density plot ages** Two populations 311 ± 35 (n=3) **364 ± 38 (n=3)**<br>**ESR/U-series isochron age** Two populations Non calculable (n=3) **≈366 (n=3)** |
| | **SN1002** | cement<br>dentine<br>enamel | 1153 ± 20 | -0.549 ± 0.106<br>-0.518 ± 0.111<br>-0.250 ± 0.150 | 584 ± 233 | 1170 ± 329 | 1560 ± 150 | 3304 ± 430 | **349 ± 45** | |
| | ***SN0902*** | *cement*<br>*dentine*<br>*enamel* | *1193 ± 45* | *-0.0038 ± 0.0001*<br>*-0.0025 ± 0.0001*<br>*-0.0015 ± 0.0001* | *605 ± 160* | *1072 ± 223* | *1560 ± 150* | *3237 ± 313* | ***369 ± 33*** | |
| | ***SN0906*** | *dentine*<br>*enamel* | *815 ± 26* | *-0.0042 ± 0.0001*<br>*-0.0044 ± 0.0001* | *438 ± 122* | *563 ± 96* | *1560 ± 150* | *2554 ± 216* | ***319 ± 25*** | |
| | ***SN1003*** | *dentine*<br>*enamel* | *698 ± 74* | *-0.0037 ± 0.0001*<br>*-0.0033 ± 0.0001* | *128 ± 272* | *283 ± 126* | *1560 ± 150* | *1971 ± 335* | ***354 ± 47*** | |
| | ***SN1004*** | *dentine*<br>*enamel* | *887 ± 45* | *-0.0035 ± 0.0004*<br>*-0.0028 ± 0.0004* | *204 ± 107* | *605 ± 172* | *1560 ± 150* | *2365 ± 227* | ***373 ± 35*** | |
| **Isernia la Pineta** (Shao et al., 2011) | **IS0901** | cement<br>dentine<br>enamel | 1645 ± 113 | 0.071 ± 0.167<br>0.385 ± 0.210<br>0.743 ± 0.256 | 448 ± 37 | 1264 ± 76 | 1910 ± 50 | 3622 ± 99 | **456 ± 54** | **$^{40}Ar/^{39}Ar$ age X < 584 ± 5**<br>**ESR/U-series density plot ages** 435 ± 48 (n=3)<br>**ESR/U-series isochron age ≈585 (n=3)** |
| | **IS0902** | dentine<br>enamel | 1238 ± 61 | 0.323 ± 0.184<br>0.362 ± 0.187 | 401 ± 28 | 713 ± 43 | 1990 ± 50 | 3104 ± 71 | **400 ± 42** | |
| | **IS0903** | cement<br>dentine<br>enamel | 1360 ± 88 | 1.275 ± 0.343<br>1.796 ± 0.413<br>2.200 ± 0.466 | 284 ± 30 | 888 ± 66 | 1720 ± 50 | 2892 ± 88 | **471 ± 59** | |
| | **IS0904** | cement<br>dentine<br>enamel | 1455 ± 89 | -0.551 ± 0.072<br>0.563 ± 0.206<br>0.599 ± 0.209 | 321 ± 23 | 1043 ± 42 | 1945 ± 50 | 3309 ± 69 | **441 ± 46** | |
| **Venosa Notarchirico** (this work) | **VN1201** | dentine<br>enamel | 751 ± 20 | -1.000<br>-0.151 ± 0.282 | 445 ± 127 | 2075 ± 546 | 1092 ± 55 | 3612 | **208 ± 32** | **$^{40}Ar/^{39}Ar$ 612 ± 4 < X < 658 ± 8**<br>**ESR/U-series density plot ages** Non calculable<br>**ESR/U-series isochron age ≈** 134 (n=3) |
| | **VN1202** | dentine<br>enamel | 1596 ± 77 | 0.479 ± 0.217<br>1.475 ± 0.344 | 1128 ± 327 | 701 ± 165 | 1092 ± 55 | 2921 ± 370 | **546 ± 64** | |
| | ***VN1203*** | *cement*<br>*dentine*<br>enamel | *2078 ± 79* | *-0.0044 ± 0.0006*<br>*-0.0045 ± 0.0006*<br>-0.898 ± 0.024 | *2352 ± 487* | *3402 ± 502* | *1092 ± 55* | *6836 ± 702* | ***304 ± 29*** | |
| | ***VN1204*** | *dentine*<br>*enamel* | *1889 ± 80* | *-0.0029 ± 0.0003*<br>*-0.0032 ± 0.0003* | *2026 ± 329* | *1350 ± 200* | *1092 ± 55* | *4477 ± 389* | ***422 ± 32*** | |
| **Isoletta** (Pereira et al., 2018) | ***ISOL1401*** | dentine<br>*enamel* | *1151 ± 33* | -0.578 ± 0.063<br>*-0.0031 ± 0.0004* | *553 ± 125* | *1063 ± 194* | *1494 ± 150* | *3110 ± 275* | ***370 ± 31*** | **$^{40}Ar/^{39}Ar$ age 374 ± 4** |
| **Valle Giumentina** (this work) | **VG1501** | dentine<br>enamel | *1577 ± 51* | *-0.0027 ± 0.0002*<br>*-0.0027 ± 0.0002* | *405 ± 110* | *800 ± 175* | *2307 ± 150* | *3512 ± 254* | ***449 ± 29*** | **$^{40}Ar/^{39}Ar$ age X < 455 ± 3** |

283 **Table 5** – ESR/U-series data and ages for the analysed teeth recovered from several Middle Pleistocene Italian sites.

284 The equivalent doses $D_E$ were extrapolated from the obtained dose-response data sets using either The growth curves were built

285 for each sample using different fitting functions (single saturating exponential, SSE, according with Apers et al., 1981;double

saturating exponential function (DSE), according with Duval et al. (2009), or exponential plus linear function ( E+L), according with Shao et al. (2015a). The equivalent dose corresponding to the function that best describes the experimental data and gives the best statistics is then used to calculate age.

The radioelement contents of sediment samples associated to each tooth were determined by in laboratory high resolution low background gamma spectrometry and *in situ* gamma measurements with TL $Al_2O_3$ dosimeters at La Polledrara and Inspector 1000 Canberra gamma spectrometer on the other sites. A sediment water content value of 15 ± 5 % was therefore assumed for the age calculations. The cosmic dose rate was estimated using the formula of Prescott and Hutton (1994). Were also used the following parameters: a k-value (α efficiency) of 0.13 ± 0.02 (Grün and Katzenberger-Apel, 1994); water content of 0 wt% in the enamel and 7 wt% in the dentine and cementum; conversion contents-doses factors from Guérin et aL; (2011). For each dental tissue, Rn loss was estimated from both gamma and alpha/ICP measurements (Bahain et al., 1992). The beta dose contributions were corrected from the enamel part destroyed on each side of the enamel layer during the preparation process (according to Brennan et al., 1997).

ESR/U-series ages, different dose-rate contributions and U-uptake parameters were then calculated using either US model (Grün et al., 1988) or AU model (Shao et al., 2012). The “USESR”, “AUESR” and “combined ESR” computer programs were used for the age calculation in which the age uncertainty (1σ) is calculated with Monte Carlo approach (Shao et al., 2014).

Isochron age estimates were newly determined in the present work except for La Polledrara samples (Pereira et al., 2017).

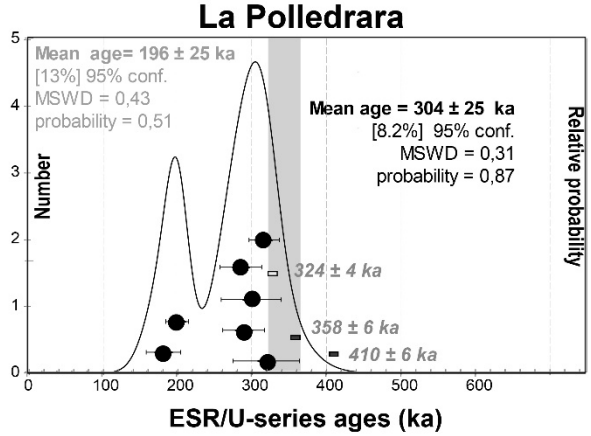
La Polledrara
Mean age= 196 ± 25 ka
[13%] 95% conf.
MSWD = 0,43
probability = 0,51
Mean age = 304 ± 25 ka
[8.2%] 95% conf.
MSWD = 0,31
probability = 0,87
Number
Relative probability
324 ± 4 ka
358 ± 6 ka
410 ± 6 ka
ESR/U-series ages (ka)

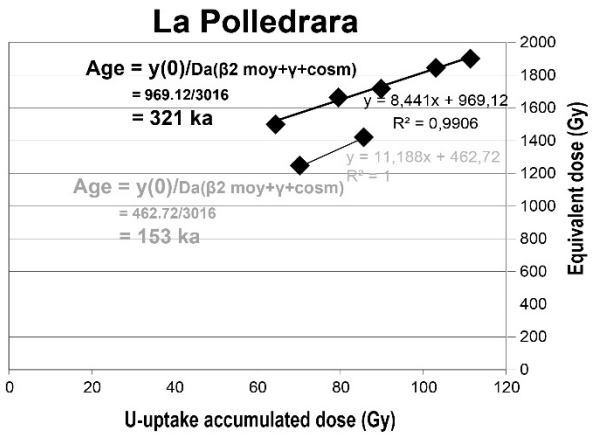
La Polledrara
Age = y(0)/Da(β2 moy+γ+cosm)
= 969.12/3016
= 321 ka
y = 8,441x + 969,12
R² = 0,9906
y = 11,188x + 462,72
R² = 1
Age = y(0)/Da(β2 moy+γ+cosm)
= 462.72/3016
= 153 ka
Equivalent dose (Gy)
U-uptake accumulated dose (Gy)

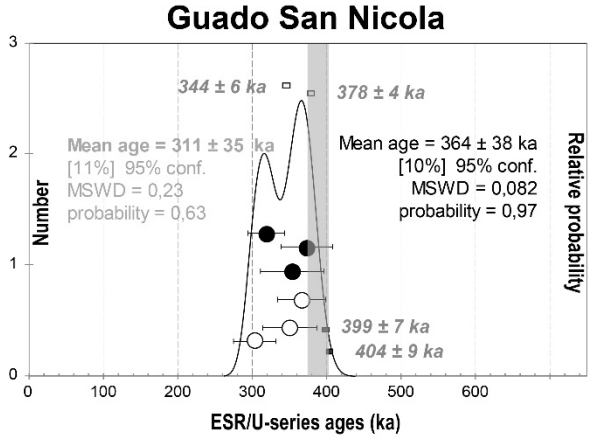
Guado San Nicola
344 ± 6 ka
378 ± 4 ka
Mean age = 311 ± 35 ka
[11%] 95% conf.
MSWD = 0,23
probability = 0,63
Mean age = 364 ± 38 ka
[10%] 95% conf.
MSWD = 0,082
probability = 0,97
Number
Relative probability
399 ± 7 ka
404 ± 9 ka
ESR/U-series ages (ka)

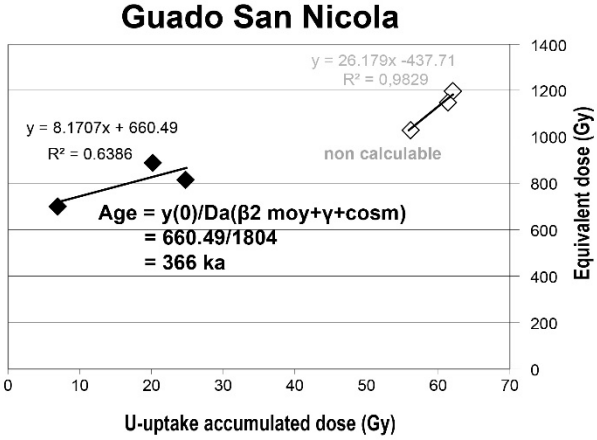
Guado San Nicola
y = 26.179x -437.71
R² = 0,9829
y = 8.1707x + 660.49
R² = 0.6386
non calculable
Age = y(0)/Da(β2 moy+γ+cosm)
= 660.49/1804
= 366 ka
Equivalent dose (Gy)
U-uptake accumulated dose (Gy)

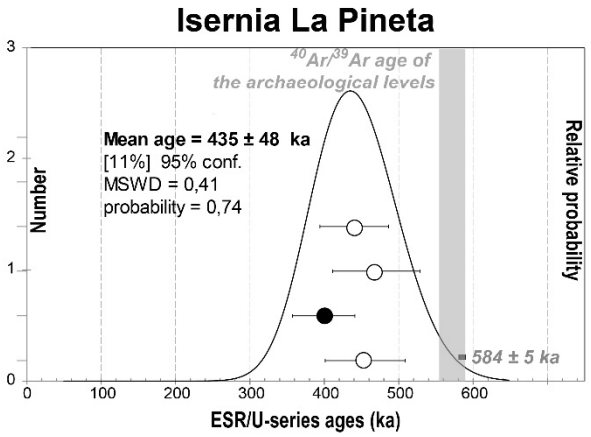
Isernia La Pineta
40Ar/39Ar age of
the archaeological levels
Mean age = 435 ± 48 ka
[11%] 95% conf.
MSWD = 0,41
probability = 0,74
Number
Relative probability
584 ± 5 ka
ESR/U-series ages (ka)

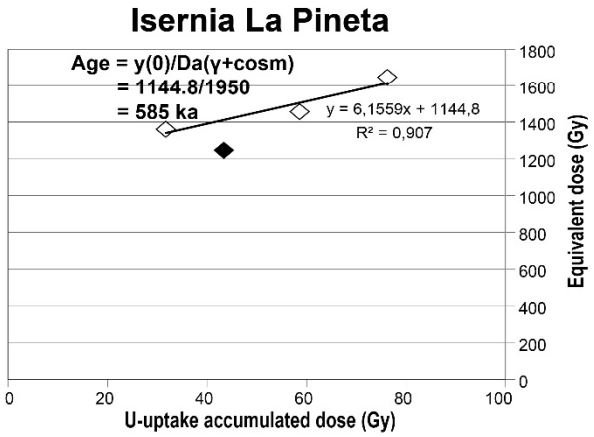
Isernia La Pineta
Age = y(0)/Da(γ+cosm)
= 1144.8/1950
= 585 ka
y = 6,1559x + 1144,8
R² = 0,907
Equivalent dose (Gy)
U-uptake accumulated dose (Gy)

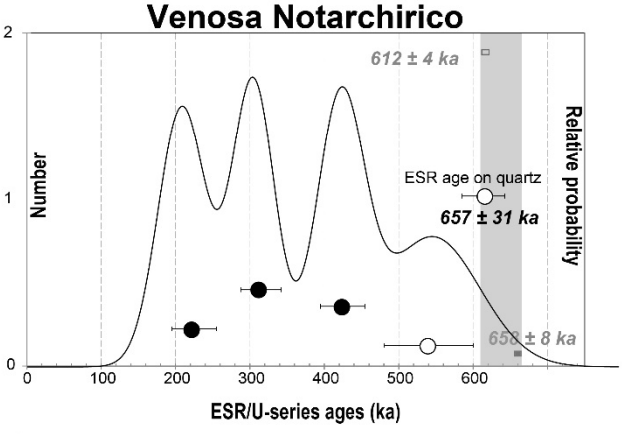
Venosa Notarchirico
612 ± 4 ka
ESR age on quartz
657 ± 31 ka
Number
Relative probability
ESR/U-series ages (ka)

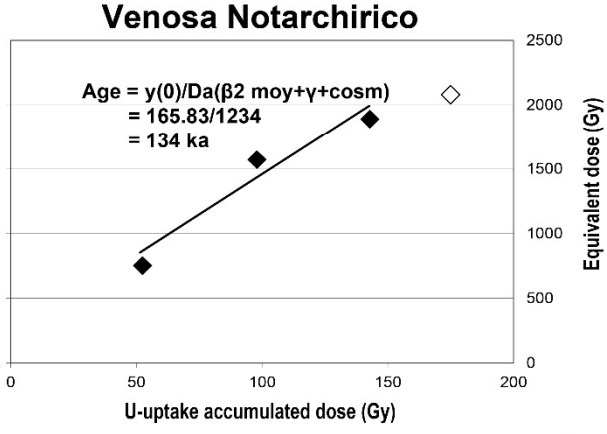
Venosa Notarchirico
Age = y(0)/Da(β2 moy+γ+cosm)
= 165.83/1234
= 134 ka
Equivalent dose (Gy)
U-uptake accumulated dose (Gy)

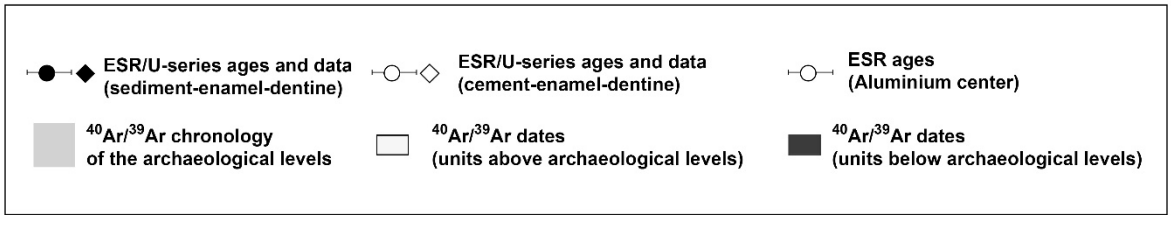
ESR/U-series ages and data
(sediment-enamel-dentine)
ESR/U-series ages and data
(cement-enamel-dentine)
ESR ages
(Aluminium center)
40Ar/39Ar chronology
of the archaeological levels
40Ar/39Ar dates
(units above archaeological levels)
40Ar/39Ar dates
(units below archaeological levels)

**Figure 3 –** Age density probability plots (left, built using Isoplot 3.0 software, Ludwig, 2003) and isochron plots (right) obtained for the different studied Middle Pleistocene sites of Central and Southern Italy with indication of the corresponding $^{40}Ar/^{39}Ar$ chronology. The U-uptake accumulated dose corresponds to the sum of the internal (enamel) and beta dose (corresponding to dentine and eventually cement) reconstructed for the considered sample all along its geological history from the modelled uptake parameters.

La Polledrara di Cecanibbio

According with the $^{40}Ar/^{39}Ar$ dates, the age of the teeth from La Polledrara di Cecanibbio upper archaeological level should be close to 324 ± 4 ka, since the altered pumices extracted from this level are geologically contemporaneous of the animal death and associated archaeological remains. The age density plot obtained using the ESR/U-series results is bimodal and the ages are variably (1-43%) underestimated. It was interpreted in previous paper as reflecting a poor dosimetric reconstruction of the internal dose rate evolution, in relation with the high U-content measured in the different dental tissues of the analysed teeth (Pereira et al., 2017). However, it should be noticed for part of the teeth that the isochron curves provide generally an age close to the $^{40}Ar/^{39}Ar$ estimates, especially for teeth without cement, that seems indicate that the measured external doses are well representative to the received historical dose. The isochron age (321 ka) obtained for 5 of the 7 analysed teeth, is similar than the oldest age mode obtained for the teeth of this site and is coherent with the $^{40}Ar/^{39}Ar$ age of this specific volcanic event. On the other hand, the isochron plot built from the apparent younger teeth population provide severely underestimated date that could reflect the record of an event posterior to the archaeological sequence deposition, such as the opening of the present-day landscape, which would lead to a drastic change of the dosimetric environmental conditions for these teeth.

Isoletta – At Isoletta, three layers were dated by $^{40}Ar/^{39}Ar$ (Pereira et al., 2018). The age of the volcanic layer in which ESR 1 quartz sample was collected is 402 ± 4 ka, while the level corresponding to ESR 4 sample, at the top of the sequence, gives an age of 364 ± 9 ka.

The ESR results obtained for Isoletta sediments are consistent within 1σ with this $^{40}Ar/^{39}Ar$ chronology, except for ESR1 sample for which severe overestimation is observed whatever the center used, due probably to both an incomplete initial bleaching of these ESR centers and a poor dose rate evaluation (Voinchet et al., 2020). Two samples (ESR4 and ESR3) provided similar ages for the three centers while the age obtained using Ti-H center is underes-

timated for ESR2 sample. Voinchet et al. (2020) suggest that Ti–H center cannot be used to determine reliable $D_E$ estimates higher than 300–400 Gy due to signal saturation, explaining such underestimation. Weighted mean ages of 442 ± 58 ka (ESR2, 2σ, Full external error, MSWD = 0.65 and P = 0.42), 349 ± 26 ka (ESR 3, 2σ, full external uncertainty, MSD = 2.08 and P = 0.059) and 396 ± 41 ka (ESR 4, 2σ, full external error, MSWD = 0.27 and P = 0.76) were obtained for these 3 sediments. The ESR/US age estimate obtained for Isoletta tooth sample, 370 ± 31 ka, agrees with both ESR dates from overlying and underlying sediments and similar to the $^{40}Ar/^{39}Ar$ age of this archaeological level, 374 ± 4 ka.

Lademagne - At Lademagne, $^{40}Ar/^{39}Ar$ chronology places the age of the archaeological levels between 404 ± 6 ka (Lad inf) and 388 ± 6 ka (Lad sup), providing hence a *terminus ante quem* for the level dated by ESR (Pereira et al., 2018). The ESR ages calculated from Ti-Li (398± 51 ka) and Al (406± 51 ka) signals are consistent, yielding a weighted mean age of 402 ± 71 ka (2σ, Full external error, MSWD = 0.012 and P = 0.91).

Guado San Nicola – . The $^{40}Ar/^{39}Ar$ data obtained chronologically place the human occupations between 404 ± 9 ka and 378 ± 4 ka (Pereira et al., 2016), a result considered then quite surprising in relation with the occurrence of Mode 3 archaeological artefacts in these levels. Here again, the age density plots built from ESR/U-series results is bimodal and the age underestimation, 1-20% lower than the $^{40}Ar/^{39}Ar$ ages, was interpreted in previous paper as related with the high U-content measured in the different dental tissues of the analysed teeth (Pereira et al., 2016). The isochron age derived from the teeth without cement, around 365 ka, is however close from the older ESR/U-series age population, 364 ± 38 ka, and, taking into account uncertainties associated with this result, in agreement with the $^{40}Ar/^{39}Ar$ age of the overlying volcanic deposit (S.U. A, 378 ± 4 ka). In contrast, the isochron plot built from the teeth with cement population does not allow any age determination.

Valle Giumentina - The $^{40}Ar/^{39}Ar$ chronology obtained for the Valle Giumentina sequence, previously supposed contemporaneous with the Rissian Glacial stage (MIS 6-8, Demangeot and Radmilli, 1953), indeed covers two glacial/interglacial cycles from MIS 15 to MIS 12 (see discussions in Nicoud et al., 2016 ; Villa et al., 2016 ; Limondin-Lozouet et al., 2017). The ESR/U-series age obtained for the tooth carried out from Acheulean ALB level, 449 ± 29 ka, is undistinguishable from the $^{40}Ar/^{39}Ar$ age of LABM level located just below, 455 ± 3 ka.

Isernia La Pineta – A primary fallout tephra layer located just below the main archaeological level t3a was dated by $^{40}Ar/^{39}Ar$ of 584 ± 5 ka (Peretto et al., 2015), furnishing a maximum age for this level. The age underestimation of ESR/U-series data is here more severe, around 25% (mean age) lower than this date. The hypothesis of a change of the external dose in relation with late uptake history in the palaeontological remains was proposed previously to

365 explain this age underestimation (Falguères et al., 2007; Shao et al., 2011), but it should be underlined that the
366 isochron age obtained for these teeth (585 ka) is in perfect agreement with the $^{40}Ar/^{39}Ar$ date .
367 Notarchirico - The situation is different at Notarchirico. For the teeth recovered from the palaeoanthropological level
368 supra α, both the ESR/US ages (ranging from 208 ± 32 ka to 546 ± 64 ka), are so scattered that it precludes any mean
369 age calculation. Isochron age estimate (134 ka) is much younger than the $^{40}Ar/^{39}Ar$ age time range estimate, dated
370 between 612 ± 4 ka and 659 ± 9 ka (Pereira et al., 2015). These results indicate that the teeth have either recently
371 experienced an event avoiding ESR/U-series dating possibilities or that the palaeodosimetric reconstruction cannot
372 be realized from present-day data. On the other hand, the ages derived from ESR analyses of Notarchirico sediments
373 are quite coherent despite the fact than only the Al center was usable. The obtained ESR age (657 ± 31 ka) agrees at
374 1σ with the $^{40}Ar/^{39}Ar$ age estimate for this level, constrained between 658 and 612 ka.
375
376 **Discussion**
377 The main purpose of the present paper was to discuss of the chronologies established by ESR and ESR/U-series
378 methods on sediments and teeth sampled for various Middle Pleistocene sites of Central and Southern Italy, display-
379 ing into their stratigraphic sequences also volcanic materials dated by $^{40}Ar/^{39}Ar$ on single grains. The figure 4 summa-
380 rizes the whole set of data obtained on the studied sites.
381 $^{40}Ar/^{39}Ar$ method was then used as reference method to provide independent chronological data on the studied
382 archaeological sites. $^{40}Ar/^{39}Ar$ results permit hence to place with confidence the studied sites in a single precise and
383 coherent chronological framework. The site succession from the youngest to the older is the following: La Polledrara
384 di Cecanibbio < Guado San Nicola ≈ Isoletta ≈ Lademagne < Valle Giumentina < Isernia la Pineta < Notarchirico. This
385 succession is slightly different than the biochronological succession previously proposed for these sites and in which
386 Isernia was supposed equivalent in age or slightly older than Notarchirico (Sardella et al., 2006; Palombo and Sar-
387 della, 2007; Marra et al., 2014). From the archaeological point of view, this chronology ranges the deposition of the
388 long stratigraphic sequence of Valle Giumentina from MIS 15 to MIS 12, while it was considered as coeval with the
389 Rissian Glacial stage (MIS 6-8, Demangeot and Radmilli, 1953). Moreover $^{40}Ar/^{39}Ar$ data indicate that the archaeolog-
390 ical levels of Guado San Nicola, in which Mode 3 lithic industry was recovered, are contemporaneous with the MIS
391 11 and 10 periods, placing the site among the oldest occurrences of this type of lithic technology (Peretto et al.,
392 2014, 2016).
393

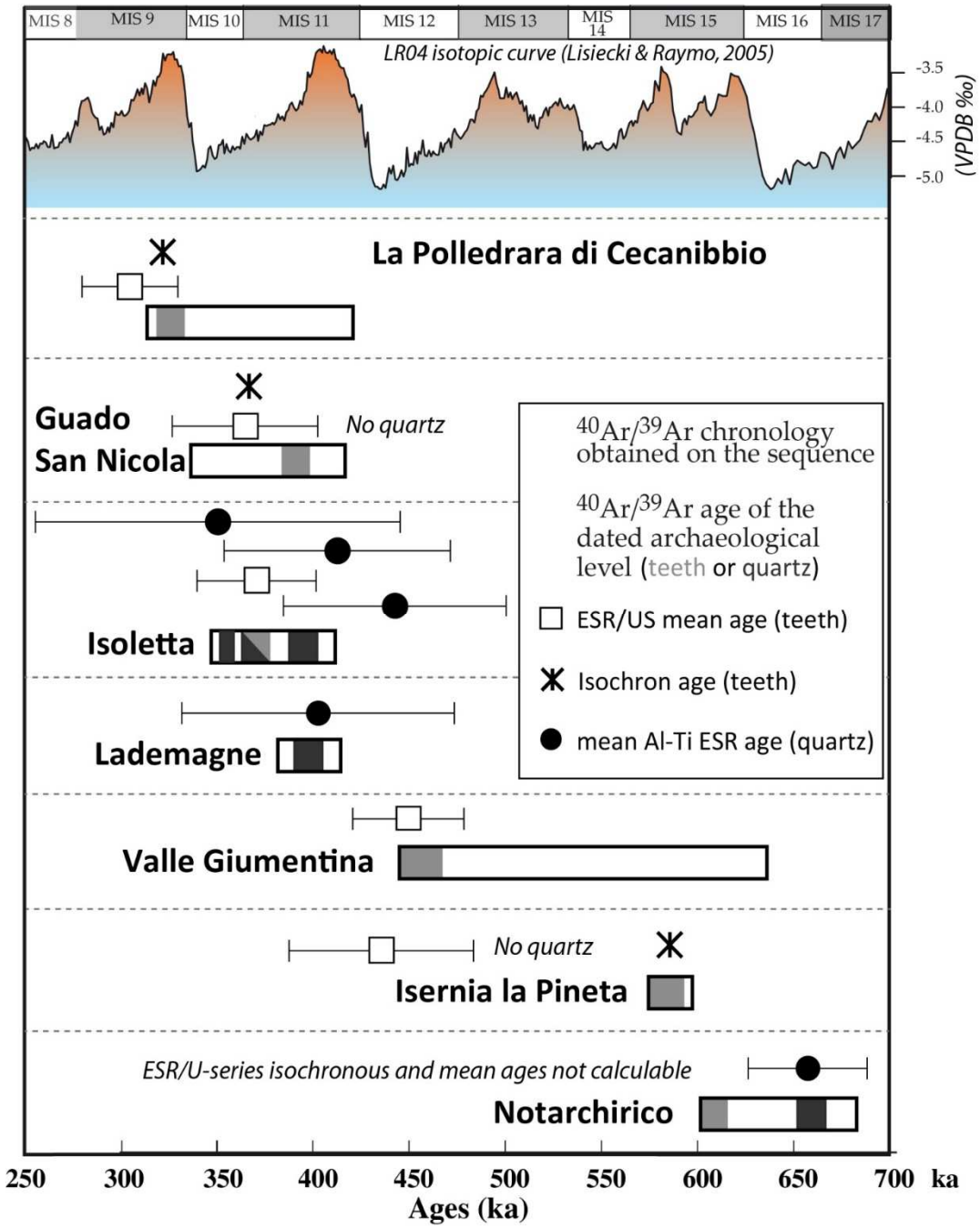


**Figure 4 –** ESR and ESR/U-series ages obtained for the different studied Middle Pleistocene sites of Central and Southern Italy with indication of the corresponding $^{40}Ar/^{39}Ar$ chronology.

The ESR ages obtained on the fluvial quartz grains are globally in agreement with these $^{40}Ar/^{39}Ar$ chronologies on the studied sites. The results derived from Al and Ti-Li ESR centers are globally similar for the main part of the analysed samples, while equivalent doses and ages obtained using Ti-H center are systematically underestimated, perhaps in relation with a faster saturation of these centers. Voinchet et al. (2020) recommend hence that Ti-H centers should not be used to date samples with equivalent doses greater than ca 300 Gy. These authors underline also that, if Al-center use can provide overestimated age estimate in case of uncomplete initial bleaching, Ti-Li center measurement can be complicated for samples displaying poor signal-to-noise resolution (Voinchet et al., 2020).

On the other hand, the ages obtained from ESR/U-series results for the different studied sites in which several teeth were analysed appear quite systematically underestimated. This underestimation is slight for the main part of the teeth recovered from the two younger sites (< 450 ka, La Polledrara and Guado San Nicola), but more drastic for the whole set of teeth carried out from the two older ones (Isernia and Notarchirico) despite very different U-uptake histories (systematic late uptake at Isernia and early uptake or leaching at Notarchirico). The use of the isochron approach attests however of the quite good reliability of the palaeodosimetric reconstruction for these different sites and the observed age underestimation could therefore be related to an underestimation of the equivalent dose. In such context, it should also be underlined that the results obtained for the single teeth from Isoletta and Valle Giumentina are in agreement with the $^{40}Ar/^{39}Ar$ ages of the dated levels.

An explanation advanced to explain such age underestimation could be linked to the high U contents recorded in some of the analysed teeth enamels and associated high internal doses reconstruction. The possibility of an inverse correlation between the uranium concentration and ESR signal intensities in enamel displaying high U content was indeed postulated, considering than the crystal lattice of the enamel could locally be completely destroyed by alpha radiations emitted by uranium decay and so that the measured ESR signal corresponds only to low uranium area (Bahain et al., 1992). This assumption has however never been demonstrated and the results of the present study indicate that, if such effect could exist, it cannot explain the whole set of data obtained in the present study. Indeed, the association of high U content in enamel, low $D_E$ value and leaching evidence in the different dental tissues (corresponding to high $^{230}Th/^{234}U$ ratios) leads to more or less severe age underestimation.

Another possible explanation of such age underestimation is linked to the fact that ESR signal of enamel is indeed resulting of several $CO_2^-$ radicals having different stabilities (Joannes Boyau and Grün, 2009). These radicals are indistinguishable from each other when working on powders as during the present study, but can be distinguished by analyses of enamel fragments (Joannes Boyau et al., 2010; see also discussion in Joannes Boyau, 2013 and references therein). Some of these radicals are unstable considering geological time range and are considered as responsible for an underestimation of up to 30% of $D_E$ values (Joannes Boyau and Grün, 2011). The equivalent doses derived from T1-B2 peak-to-peak measurements could therefore be affected by this lower stability of these unstable $CO_2^-$ radicals to a greater or lesser degree. It could be also dependant on the dose rate intensity, complicating for the moment the taking into account of this parameter. Systematic comparisons between powder and enamel fragment ESR studies could allow a better estimation of the impact of this poor stability but it necessitates specific ESR equipment and is very time consuming. As the isochron plots provide results in agreement for part of the studied teeth sets, it seems

that an reliable age estimate can be obtained by this way if the dose rate has not changed over the geological history of the site in question. Here also, such assumption will have to be confirmed by subsequent studies. It could be also interesting to rely powder and fragment studies as well to try to characterize the relative percentages of stable and unstable $CO_2^-$ radicals in ESR powder spectra to correct for each sample a possible $D_E$ underestimation. Unfortunately, such studies are still scarce and the various methods proposed to such correction were not sufficiently checked with independent age control and systematic corrections seem thus to be premature (see details in Joannes Boyau, 2013).

Despite these questions, the results obtained in the present study are encouraging and pemitted to clarify the chronology of the early Middle Pleistocene prehistoric sites in Italy, ranging approximately between 300 and 700 ka. We are currently trying to apply to other site the same multi-method approach associating ESR and ESR/U-series with independent radiisotopic methods ($^{40}Ar/^{39}Ar$, but also U-series, $^{14}C$ and other cosmonuclides) s, either more recent (late Middle Pleistocene and Upper Pleistocene) or older (Lower Pleistocene).

**Conclusions**

The ESR and combined ESR/U-series ages determined from analyses realized respectively on quartz and teeth carried out from several Middle Pleistocene Italian sites were systematically compared with $^{40}Ar/^{39}Ar$ ages obtained on K-feldspars minerals derived from volcanic or fluvial deposits. The ESR/U-series ages seem quite systematically underestimated (from 1 to 66 % depending on the age of the sites) but the isochron age estimates obtained on three sites are in agreement with the corresponding $^{40}Ar/^{39}Ar$ chronologies and indicate that the palaeodosimetric reconstruction is generally correct for the dated levels, with the notable exception of Notarchirico site. For the quartz ESR dating, the multi-center approach was used when possible. The ages determined both from Ti-Li and Al signals are generally in agreement with each other and consistent with the $^{40}Ar/^{39}Ar$ ages, while the Ti-H age estimates appear as underestimated for samples associated to $D_E$ values higher than 300 Gy, suggesting a saturation of the Ti-H traps in these samples (Voinchet et al., 2020).

These results are overall encouraging and pinpoints the necessity when possible to cross-check the methods as well to analyse several samples by dated level. At Notarchirico, both ESR/U-series and isochron ages are much younger than the expected age, by contrast with the ESR age which is in good agreement with the $^{40}Ar/^{39}Ar$ ages. Lastly, at Isoletta, both ESR/U-series, ESR and $^{40}Ar/^{39}Ar$ are in good agreement. These data indicate also that the

ESR/U-series and ESR chronologies established on Western European Palaeolithic sites when other independent methods are not available reflect rather well the geological ages of the dated Middle Pleistocene levels.

**Acknowledgements**

We would like to express our gratitude to the Italian archaeologists and administrative service that allowed the realization of this study, with special thanks to Anna-Paola Anzidei †, Marta Arzarello, Daniele Aureli, Italo Biddittu, Grazia-Maria Bulgarelli Giuseppe Lembo, Brunella Muttillo, Marie-Hélène Moncel, Elisa Nicoud, Carlo Peretto, Christian Perrenoud, Marcello Piperno, Benedetto Sala and Valentina Villa for their availability, patience and helpful discussions. We want also thank the two anonymous reviewers for their constructive comments and suggestions that are permitted to greatly improve the manuscript.

The present study was financially supported by the ATM program «Les dynamiques socio-écosystèmiques, entre perturbations et résiliences environnementales et culturelles» of the MNHN (project «Acheulean and volcanism in Italy» conducted by M.-H. Moncel (CNRS) and J.-J. Bahain (MNHN)) and the PHC Galileo project no. 28237WA «l'Acheuléen en Italie méridionale: Chronologie, Paléoanthropologie, Cultures» led by J.-J. Bahain (MNHN) and C. Peretto (University of Ferrara) which allowed the funding of part of the field missions. The PhD project of Alison Pereira was financially supported by the "Ecole Française de Rome" and the "Université Franco-Italienne". Olivier Tombret has benefited from the help of the French National Research Agency, LabEx ANR-10-LABX-0003-BCDiv, within the project "Investissements d'avenir" n_ ANR-11-IDEX-0004-02.

The ESR and mobile gamma-ray spectrometers of the French National Museum of Natural History were bought with the financial support of the 'Sesame Île-de-France' program, the 'Région Centre' and the aforementioned BcDIV program respectively.

**References**

Anzidei, A.P., Arnoldus Huizendveld, A., Palombo, M.R., Argenti, P., Caloi, L., Marcolini, F., Lemorini, L., Mussi, M., 2004. Nouvelles données sur le gisement Pléistocène moyen de La Polledrara di Cecanibbio (Latium, Italie). In: Baquedano, E., Rubio, S. (Eds.), Miscelànea en homenaje a Emiliano Aguirre. Zona Archeologica 4. Archeologia. Museo Arqueológico Regional, Madrid, 20-29.

490 Anzidei, A.P., Bulgarelli, G.M., Catalano, P., Cerilli E., Gallotti R., Lemorini C., Milli S., Palombo, M.R., Pantano, W.,
491 Santucci, E., 2012. Ongoing research at the late Middle Pleistocene site of La Polledrara di Cecanibbio (central Italy),
492 with emphasis on human elephant relationships. Quaternary international 255, 171-187.

493 Apers, D., Debuyst, R., Cannière, P. de, Dejehet, F., Lombard, E., 1981. Critique de la datation par résonance parama-
494 gnétique électronique (ESR) des planchers stalagmitiques de la Caune de l'Arago. In: Lumley, H. de, Labeyrie, J. de
495 (Ed), Datations et Analyses Isotopiques en Préhistoire: Méthodes et Limites. Edition du CNRS, Paris, pp. 533-550 pre-
496 print.

497 Ascenzi, A., Biddittu, I., Cassoli, P.F., Segre, A.G., Segre Naldini, E., 1996. A calvarium of late Homo erectus from
498 Ceprano, Italy. Journal of Human Evolution 31, 409-423.

499 Bahain J.-J, Shao Q., Falguères C., Garcia T., Dolo J.-M., Douville E., Frank N., 2014. Datation du site de Guado San
500 Nicola di Monteroduni par les méthodes de la résonance de spin électronique et du déséquilibre dans les familles de
501 l'uranium combinées (ESR/U-Th). In Muttilo B., Lembo G., Peretto C. (dir), L'insediamento a bifacciali di Guado San
502 Nicola (Monteroduni, Molise, Italia), Annali dell'Università di Ferrara Museologia Scientifica e Naturalistica, 10/1, 53-
503 56

504 Bahain J.-J., Falguères C., Dolo J.-M., Antoine P., Auguste P., Limondin-Lozouet, N., Locht J.-L., Tuffreau A., 2010.
505 ESR/U-series dating of teeth recovered from well-stratigraphically age-controlled sequences from Northern France.
506 Quaternary Geochronology 5, 371-375.

507 Bahain, J.-J., Yokoyama, Y., Falguères, C., Sarcia, M.N., 1992. ESR dating of tooth enamel: a comparison with K-Ar
508 dating. Quaternary Science reviews, 11, 245-250.

509 Biddittu, I., 2004. *Guida del Museo Preistorico di Pofi*. I Quad. di ARGIL 1, 1-158.

510 Biddittu, I., Canetri, E., Comerci, V,. Germani, M., Picchi, G., 2012. Nuove ricerche nel giacimento del Paleolitico infe-
511 riore di Lademagne, S. Giovanni Incarico (Frosinone). In Ghini, G. and Mari, Z., (eds) *Lazio e Sabina*, Edizioni Quasar,
512 9, 437-443.

513 Bischoff J.L., Robert J., Rosenbauer R.J.V., 1988. A test of Uranium-series dating of fossil tooth enamel: result from
514 Tournal Cave, France. Applied Geochemistry 3, 145-151.

515 Blackwell, B.A., Schwarcz, H.P., 1993. ESR isochron dating for teeth: a brief demonstration in solving the external
516 dose calculation problem. Applied Radiation and Isotopes 44, 243-252.

Brennan, B, Lyons, R, Phillips, S. 1991. Attenuation of alpha particle track dose for spherical grains. Nuclear Tracks Radiation Measurements 18, 249-253.

Brennan, B. 2003. Beta doses to spherical grains. Radiation Measurements 37, 299- 303.

Brennan, B.J., Rink, W.J., McGuirl, E.L., Schwarcz, H.P., Prestwich, W.V., 1997. Beta doses in tooth enamel by ''One Group'' theory and the Rosy ESR dating software. Radiation Measurements 27, 307–314.

Brown F.H., McDougall I., Gathogo P.N., 2012. Age ranges of Australopithecus species, Kenya, Ethiopia and Tanzania. In Reed K.E., Fleagle J.G., Leakey R. (eds.) The Paleobiology of Australopithecus, Vertebrate Paleobiology and Paleoanthropology Series, Springer, PP 7-20.

Coltorti M, Cremaschi M, Delitalia MC, Esu D, Fornaseri M, McPherron A, Nicoletti M., Van Otterloo R., Peretto C., Sala B., Schmidt V., Sevink J. 1982. Reversed magnetic polarity at an early Lower Palaeolithic site in central Italy. Nature 300, 173–176

Dolo J.M., Lecerf N., Mihajlovic V., Falguères C., Bahain J.-J., 1996. Contribution of ESR dosimetry for irradiation of geological and archaeological samples with a 60Co panoramic source. Applied Radiation and Isotopes 47, 1419-1421

Duval M., Grün R., Falguères C., Bahain J.-J., Dolo J.-M., 2009. ESR dating of Lower Pleistocene fossil teeth: limits of the single saturating exponential (SSE) function for the equivalent dose determination. Radiation measurements 44, 477-482.

Duval, M. Grün, R., 2016. Are published ESR dose assessments on fossil tooth enamel reliable? Quaternary Geochronology 31, 19-27.

Duval, M., Guilarte, V., 2015. ESR dosimetry of optically bleached quartz grains extracted from Plio-quaternary sediment: evaluating some key aspects of the ESR signal associated to the Ti-center. Radiation Measurement 78, 28–41

Falguères, C., Bahain, J.-J., Dolo, J.-M., Mercier, N. , Valladas, H., 2007. On the interest and the limits of using combined ESR/U-series model in the case of very late uranium uptake. Quaternary Geochronology 2, 403–408.

Grün, R., 1994. A cautionary note: use of the “water content” and “depth for cosmic ray dose rate” in AGE and DATA. Ancient TL 12, 50- 51.

Grün, R., 2000. Methods of dose determination using ESR spectra of tooth enamel. Radiation Measurements 32, 767-772

543 Grün, R., Katzenberger-Apel, O., 1994. An alpha irradiator for ESR dating. Ancient TL 12, 35–38.

544 Grün, R., Schwarcz, H.P., Chadam, J.M., 1988. ESR dating of tooth enamel: coupled correction for U-uptake and U-
545 series disequilibrium. Nuclear Tracks and Radiation Measurements, 14, 237-241.

546 Guérin, G., Mercier, N., Adamiec, G., 2011. Dose-rate conversion factors: update. Ancient TL, 29, 5-8.

547 Joannes-Boyau R., 2013. Detailed protocol for an accurate non-destructive direct dating of tooth enamel fragment
548 using electron spin resonance. Geochronometria 40, 322-333.

549 Joannes-Boyau R., Grün R., 2009. Thermal behavior of oriented and non-oriented CO2- radicals in tooth enamel.
550 Radiation Measurements 44, 505-511.

551 Joannes-Boyau R., Bodin T., Grün R., 2010. Decomposition of the angular ESR spectra of fossil tooth enamel frag-
552 ments. Radiation Measurements 45, 887-898.

553 Joannes-Boyau R., Grün R, 2011. A comprehensive model for CO2- radicals in fossil tooth enamel: implications for
554 ESR dating. Quaternary Geochronology 6, 82-97.

555 Laurent, M., Falguères, C., Bahain, J-J., Rousseau, L., Van Vliet-Lanoë, B. 1998. ESR dating of quartz extracted from
556 Quaternary and Neogene sediments: method, potential and actual limits. Quaternary Science Reviews 17, 1057-
557 1061.

558 Lee, J.Y., Marti, K., Severinghaus, J.P., Kawamura, K., Hee-Soo, Y., Lee, J.B., Kim, J.S., 2006. A redetermination of the
559 isotopic abundances of atmospheric Ar. Geochimica et Cosmochimica Acta 70, 4507-4512

560 Lefèvre D., Raynal J.-P., Vernet G., Kieffer G., Piperno M., 2010. Tephro-stratigraphy and the age of ancient Southern
561 Italian Acheulean settlements: The sites of Loreto and Notarchirico (Venosa, Basilicata, Italy). Quaternary Internatio-
562 nal 223–224, 360–368

563 Limondin-Lozouet N., Villa V., Pereira A., Nomade S., Bahain J.-J., Stoetzel E., Aureli D., Nicoud E., 2017. Middle Pleis-
564 tocene molluscan fauna from Central Italy at Valle Giumentina (Abruzzo): palaeoenvironmental, biostratigraphical
565 and biogeographical implications. Quaternary Science Reviews 156, 135-149

566 Lisiecki, L.E., Raymo, M.E. 2005. A Pliocene-Pleistocene stack of 57 globally distributed benthic d18O records.
567 Paleoceanography 20, PA 1003, doi:10.1029/2004PA001071

568 Ludwig K. R., 2003. Isoplot 3.0, a geochronological toolkit for Microsoft Excel. Berkeley Geochronology Center Special
569 Publication, 4, 71p

570 McDougall I., 2014. K/Ar and 40Ar/39Ar isotopic dating techniques as applied to young volcanic rocks, particularly
571 those associated with hominin localities. In Holland H.D., Turekian K.K. (eds) Treatise on Geochemistry, 14, 1-15

572 Mallegni F., Segre A.G., Segre-Naldini E., 1991. Découverte d'un fémur acheuléen à Notarchirico (Venosa, Basilicate).
573 L'Anthropologie 95, 47-88.

574 Manzi, G. 2016. Humans of the Middle Pleistocene: The controversial calvarium from Ceprano (Italy) and its signifi-
575 cance for the origin and variability of *Homo heidelbergensis*. Quaternary International 411, 254-261.

576 Marra F., Pandolfi L., Petronio C., Di Stefano G., Gaeta M., Salari L., 2014. Reassessing the sedimentary deposits and
577 vertebrate assemblages from Ponte Galeria area (Rome, central Italy): An archive for the Middle Pleistocene faunas
578 of Europe. Earth-Science Reviews 139, 104–122.

579 Marra, F., Nomade, S., Pereira, A., Petronio, C., Salari, L., Sottili, G., Bahain, J.J., Boschian, G., Di Stefano, G.,
580 Falguères, C., Florindo, F., Gaeta, M., Giaccio, B., Masotta, M., 2018. A review of the geologic sections and the faunal
581 assemblages of Aurelian Mammal Age of Latium (Italy) in the light of a new chronostrati-graphic framework. Quater-
582 nary Science Reviews 181, 173–199.

583 Murray, A.S., Roberts, R.G., 1997. Determining the burial time of single grains of quartz using optically stimulated
584 luminescence. Earth and Planetary Science Letters 152, 163-180.

585 Niespolo, E.M., Rutte, D., Deino, A., Renne, P.R., 2017. Intercalibration and age of the Alder Creek sanidine
586 40Ar/39Ar standard. Quaternary Geochronology 39, 205-213.

587 Nomade, S., Gauthier, A., Guillou, H., Pastre, J.F., 2010. 40Ar/39Ar temporal framework for the Alleret maar lacus-
588 trine sequence (French Massif Central): Volcanological and Paleoclimatic implications. Quaternary Geochronology 5,
589 20-27.

590 Nomade, S., Renne, P.R., Vogel, N., Deino, A.L., Sharp, W.D., Becker, T.A., Jaouni, A.R., Mundil, R., 2005. Alder Creek
591 sanidine (ACs-2), A Quaternary $^{40}Ar/^{39}Ar$ dating standard tied to the Cobb Mountain geomagnetic event. Chemical
592 Geology 218, 315–338.

593 Palombo M.R., Sardella R., 2007. Biochronology and biochron boundaries: A real dilemma or a false problem? An
594 example based on the Pleistocene large mammalian faunas from Italy Quaternary International 160, 30–42.

595 Pereira A., Nomade S., Falguères C., Bahain J.-J., Tombret O., Garcia T., Voinchet P., Bulgarelli G.-M., Anzidei A.-P.,
596 2017. New $^{40}Ar/^{39}Ar$ and ESR/U-series data for the La Polledrara di Cecanibbio archaeological site (Lazio, Italy). Jour-
597 nal of Archaeological Science: Reports 15, 20-29.
598 Pereira A., Nomade S., Moncel M.-H., Voinchet P., Bahain J.-J., Biddittu I., Falguères C., Giaccio B., Manzi G., Parenti
599 F., Scardia G., Scao V., Sottili G., Vietti A. , 2018. Integrated geochronology of Acheulian sites from the southern Lati-
600 um (central Italy): Insights on human-environment interaction and the technological innovations during the MIS 11-
601 MIS 10 period. Quaternary Science Reviews 187, 112-129.

602 Pereira A., Nomade S., Shao Q., Bahain J.-J., Arzarello M., Douville E., Falguères C., Frank N., Garcia T., Lembo G.,
603 Muttillo B., Peretto C., 2016. 40Ar/39Ar and ESR-U/Th dates for Guado San Nicola, Middle Pleistocene key site at the
604 Lower/Middle Palaeolithic transition in Italy. Quaternary Geochronology, 36, 67-75

605 Pereira A., Nomade S., Voinchet P., Bahain J.-J., Falguères C., Garon H., Lefèvre D., Raynal J.-P., Scao V., Piperno M.,
606 2015. The earliest securely dated hominid fossil in Italy and evidences of Acheulian human occupations during glacial
607 MIS 16 at Notarchirico (Venosa, Basilicata, Italy). Journal of Quaternary Science, 30 (7), 639-650

608 Peretto C., Arnaud J., Moggi-Cecchi J., Manzi G., Nomade S., Pereira A., Falguères C., Bahain J.-J., Grimaud-Hervé D.,
609 Berto C., Sala B., Lembo G., Muttillob., Gallotti R., Thun Hohenstein U., Vaccaro C., Coltorti M., Arzarello M., 2015. A
610 Human Deciduous Tooth and New 40Ar/39Ar Dating Results from the Middle Pleistocene Archaeological Site of
611 Isernia La Pineta, Southern Italy. PLoS ONE, 10 (10), e0140091

612 Peretto C., Arzarello M., Bahain J.-J., Boulbes N., Coltorti M., Dolo J.-M., Douville E., Falguères C., Frank N., Garcia T.,
613 Lembo G., Moigne A.-M., Muttillo B., Nomade S., Shao Q., Pereira A., Pieruccini P., Rufo M.A., Sala B., Thun Hohen-
614 stein U., Tessari U., Turrini M.C., Vaccaro C., 2016. The Middle Pleistocene site of Guado San Nicola (Monteroduni,
615 Central Italy) on the Lower/Middle Palaeolithic transition. Quaternary International 411, 301-315

616 Peretto C., Terzani C., Cremaschi M., 1983. Isernia la Pineta : un accampamento piu antico di 700.000 anni. Calderine
617 editore, Bologne.

618 Peretto, C., Arzarello, M., Bahain, J.J., Boulbes, Coltorti, M., De Bonis, A., N., Douville, E., Falguères, C., Frank, N.,
619 Garcia, T., Lembo, G., Moigne, Morra, V., A.M., Muttillo, B., Nomade, S., Shao, Q., Perrotta, A., Pieruccini, P., Rufo,
620 M., Sala, B., Scarpati, C., Thun Hohenstein, U., Tessari, U., Turrini, M.C., Vaccaro, C. 2014. L'occupazione umana del

621 Pleistocene medio di Guado San Nicola (Monteroduni, Molise). Annali dell'Università di Ferrara, Museologia
622 Scientifica e Naturalistica 10, 23-31.

623 Petronio C., Di Stefano G., Kotsakis T., Salari L., Marra F., Jicha B.R., 2019. Biochronological framework for the late
624 Galerian and early-middle Aurelian Mammal Ages of peninsular Italy. Geobios, 53, 35–50 .

625 Piperno M. 1997. Notarchirico, un sito del Pleistocene medio iniziale nel bacino di Venosa, Osanna Venosa (eds),
626 Venosa.

627 Prescott, J.R., Hutton, J.T., 1994. Cosmic ray contributions to dose rates for luminescence and ESR dating: large
628 depths and long-term time variations. Radiation Measurements, 23, 497–500.

629 Renne, P.R., Mundil, R., Balco, G., Min, K., Ludwig, K.R., 2011. Response to the comment by W.H. Schwarz et al. on
630 "Joint determination of 40K decay constants and 40Ar∗/40K for the Fish Canyon sanidine standard, and improved
631 accuracy for 40Ar/39Ar geochronology" by P.R. Renne et al. (2010). Geochimica Cosmochimica Acta 75, 5097-5100

632 Santucci, E., Marano, F., Cerilli, E., Fiore, I., Lemorini, C., Palombo, M.R., Anzidei, A.P., Bulgarelli, G.M., 2016. *Palae-*
633 *oloxodon* exploitation at the Middle Pleistocene site of La Polledrara di Cecanibbio (Rome, Italy). Quaternary
634 international 406 part B, 169-182. .

635 Sardella R., Palombo M.R., Petronio C., Bedetti C., Pavia M., 2006. The early Middle Pleistocene large mammal fau-
636 nas of Italy: An overview. Quaternary International 149, 104–109.

637 Shao, Q., Bahain, J.-J., Falguères, C., Peretto, C., Arzarello, M., Minelli, A., Hohenstein, U.T., Dolo, J.-M., Garcia, T.,
638 Frank, N., Douville, E., 2011. New ESR/U-series data for the early middle Pleistocene site of Isernia la Pineta, Italy.
639 Radiation Measurements 46, 847-852.

640 Shao, Q., Bahain, J.-J., Falguères, C.., Dolo, J.-M., Garcia, T., 2012. A new U-uptake model for combined ESR/U-series
641 dating of tooth enamel. Quaternary Geochronology, 10, 406-411.

642 Shao, Q., Bahain, J.-J., Dolo, J.M., Falguères, C., 2014. Monte Carlo approach to calculate US-ESR ages and their un-
643 certainties. Quaternary Geochronology 22, 99-106.

644 Shao Q., Bahain J.-J., Wang W., Jin C., Wang Y., Voinchet P., Lin M., 2015a. Combined ESR and U-series dating of early
645 Pleistocene Gigantopithecus faunas at Mohui and Sanhe Caves, Guangxi, southern China. Quaternary Geochronolo-
646 gy, 30, 524-528

Shao Q., Chadam J., Grün R., Falguères C., Dolo J.-M., Bahain J.-J., 2015b. The mathematical basis for the US-ESR dating method. Quaternary Geochronology 30, 1-8

Steiger, R.H., Jäger, E., 1977. Subcommission on geochronology: convention on the use of decay constants in geo- and cosmochronology. Earth and Planetary Science Letters 6, 359-362.

Tissoux, H., Voinchet, P., Lacquement, F., Prognon, F., Moreno, D., Falguères, C., Bahain, J.-J., Toyoda S. 2013. Investigation on non-optically bleachable components of ESR aluminium signal in quartz. Radiation Measurements, 47, 9, 894-899.

Toyoda, S., Voinchet, P., Falguères, C., Dolo, J.M., Laurent, M., 2000. Bleaching of ESR signal by the sunlight: a laboratory experiment for establishing the ESR dating of sediments. Applied Radiation Isotopes, 52, 5, 1357–1362.

Toyoda, S., Falguères C., 2003. The method to represent the ESR signal intensity of the aluminium hole center in quartz for the purpose of dating. Advances in ESR applications, 20, 7-10.

Vandenbergue, D., De Corte, F., Buylaert J.P., Kucera, J., Van den haute, P., 2008. On the internal radioactivity in quartz. Radiation Measurements 43, 771-775.

Voinchet, P., Bahain, J.J., Falguères, C., Laurent, M., Dolo, J.M., Despriée, J., Gageonnet, R., Chaussé, C., 2004. ESR dating of Quartz extracted from Quaternary sediments: application to fluvial terraces system of Northern France. Quaternaire 15, 135-142.

Voinchet, P., Yin, G., Falguères, C., Liu, C., Fei, H., Sun, X., Bahain, J.J., 2013. ESR dose response of the Al center measured in quartz samples from the Yellow River (China): implications for the dating of Upper Pleistocene sediment. Geochronometria 40, 341–347.

Voinchet, P., Pereira, A., Nomade, S., Falguères, C., Biddittu, I., Piperno, M., Moncel, M.-H., Bahain, J.-J., 2020. ESR dating applied to optically bleached quartz - a comparison with 40Ar/39Ar chronologies on Italian Middle Pleistocene sequences, Quaternary International, 556, 113-123 .

Yokoyama, Y., Falguères, C., Quaegebeur, J.P., 1985. ESR dating of quartz from Quaternary sediments: first attempts. Nuclear Tracks 10, 921-928.

673 **Figure caption**

674

675 **Figure 1** - Location of the studied Middle Pleistocene sites in Central and Southern Italy.

676

677 **Figure 2 –** Simplified stratigraphic logs of the studied Middle Pleistocene sites with indication of the levels dated by
678 $^{40}Ar/^{39}Ar$ and positions of the levels sampled for ESR and ESR/U-series studies. $^{40}Ar/^{39}Ar$ ages were obtained directly
679 on tephra levels (primary deposits) or on potassic feldspar grains extracted from fluvial sediments (secondary
680 deposits), the youngest population corresponding then to a maximum age for the dated level.

681

682 **Figure 3 –** Age density probability plots (left, built using Isoplot 3.0 software, Ludwig, 2003) and isochron plots (right)
683 obtained for the different studied Middle Pleistocene sites of Central and Southern Italy with indication of the corre-
684 sponding $^{40}Ar/^{39}Ar$ chronology. The U-uptake accumulated dose corresponds to the sum of the internal (enamel) and
685 beta dose (corresponding to dentine and eventually cement) reconstructed for the considered sample all along its
686 geological history from the modelled uptake parameters.

687

688 **Figure 4 –** ESR and ESR/U-series ages obtained for the different studied Middle Pleistocene sites of Central and
689 Southern Italy with indication of the corresponding $^{40}Ar/^{39}Ar$ chronology.

690

691 **Table caption**

692

693 **Table 1** – List and nature of the analysed teeth from several Middle Pleistocene Italian sites

694

695 **Table 2** – $^{40}Ar/^{39}Ar$ ages obtained from volcanic minerals recovered from several Middle Pleistocene Italian sites.
696 The indicated $^{40}Ar/^{39}Ar$ age corresponds to the age of the youngest homogeneous potassic feldspars population.
697 These ages were re-calculated in the present contribution according to the monitor flux standard ACs-2 at 1.1891 Ma
698 (Niespolo e al., 2017) and the K total decay constant of Renne et al. (2011) from the original data published in the
699 various referred papers. A homogeneous population is considered relevant when the weighted mean of these crys-

tals has the following statistical characteristics: MSWD < 1.5, Probability fit ≥ 0.1. The weighted average ages were calculated using IsoPlot 3.0 (Ludwig, 2003) and given at 95% (2σ) of confidence.

**Table 3** – ESR data and ages for sediments recovered from several Middle Pleistocene Italian sites.

Equivalent doses ($D_E$) were derived from the obtained intensity growth curves using an exponential + linear function for Al and Ti-Li centers (Duval et al., 2009; Voinchet et al., 2013) and by a single saturating exponential function for Ti-H from the six first points of the growth curves (Voinchet et al., 2020) with Microcal OriginPro 8 software, both with $1/I^2$ weighting (according with Yokoyama et al., 1985). Age calculations were performed using the following parameters: dose-rate conversions factors from Guérin et al. (2011); a k-value of 0.15 ± 0.1 (Laurent et al., 1998); alpha and beta attenuations from Brennan (2003) and Brennan et al. (1991); water attenuation formulae from Grün (1994); cosmic dose rate estimated from the Prescott and Hutton's equations (1994). The internal dose rate was considered as negligible because of the low contents of radionuclides usually found in quartz grains (Murray and Roberts 1997; Vandenbergue et al. 2008). ESR age estimates are given with one sigma error range.

**Table 4** – U-series and ESR data for the analysed teeth recovered from several Middle Pleistocene Italian sites.

U-series analyses were performed on each dental tissue in order to determine the U-uptake parameters necessary to the dose rate contributions and age calculations (see details in Shao et al., 2015b), either by alpha spectrometry (MNHN, Paris), or by Neptune Multi-Collector Inductively Coupled Plasma Mass Spectrometer (MC-ICPMS) (Nanjing Normal University, China).

**Table 5** – ESR/U-series data and ages for the analysed teeth recovered from several Middle Pleistocene Italian sites.

The equivalent doses $D_E$ were extrapolated from the obtained dose-response data sets using either The growth curves were built for each sample using different fitting functions (single saturating exponential, SSE, according with Apers et al., 1981;double saturating exponential function (DSE), according with Duval et al. (2009), or exponential plus linear function ( E+L), according with Shao et al. (2015a). The equivalent dose corresponding to the function that best describes the experimental data and gives the best statistics is then used to calculate age.

The radioelement contents of sediment samples associated to each tooth were determined by in laboratory high resolution low background gamma spectrometry and *in situ* gamma measurements with TL $Al_2O_3$ dosimeters at La

Polledrara and Inspector 1000 Canberra gamma spectrometer on the other sites. A sediment water content value of 15 ± 5 % was therefore assumed for the age calculations. The cosmic dose rate was estimated using the formula of Prescott and Hutton (1994). Were also used the following parameters: a k-value (α efficiency) of 0.13 ± 0.02 (Grün and Katzenberger-Apel, 1994); water content of 0 wt% in the enamel and 7 wt% in the dentine and cementum; conversion contents-doses factors from Guérin et aL; (2011). For each dental tissue, Rn loss was estimated from both gamma and alpha/ICP measurements (Bahain et al., 1992). The beta dose contributions were corrected from the enamel part destroyed on each side of the enamel layer during the preparation process (according to Brennan et al., 1997).

ESR/U-series ages, different dose-rate contributions and U-uptake parameters were then calculated using either US model (Grün et al., 1988) or AU model (Shao et al., 2012). The "USESR", "AUESR" and "combined ESR" computer programs were used for the age calculation in which the age uncertainty (1σ) is calculated with Monte Carlo approach (Shao et al., 2014).

Isochron age estimates were newly determined in the present work except for La Polledrara samples (Pereira et al., 2017).